GEOLOGY OF THE INTERMOUNTAIN WEST

an open-access journal of the Utah Geological Association

ISSN 2380-7601

Volume 7 ***2020***

FALLOUT TUFFS IN THE EOCENE DUCHESNE RIVER FORMATION, NORTHEASTERN UTAH—AGES, COMPOSITIONS, AND LIKELY SOURCE

Michael S. Jensen, Bart J. Kowallis, Eric H Christiansen, Casey Webb, Michael J. Dorais, Douglas A. Sprinkel, and Brian Jicha

GEOLOGY OF THE INTERMOUNTAIN WEST

an open-access journal of the Utah Geological Association

ISSN 2380-7601

Volume 7 ***2020***

Editors

Douglas A. Sprinkel
Azteca Geosolutions
801.391.1977
GIW@utahgeology.org
dsprinkel@gmail.com

Thomas C. Chidsey, Jr.
Utah Geological Survey
801.537.3364
tomchidsey@utah.gov

Bart J. Kowallis
Brigham Young University
801.422.2467
bkowallis@gmail.com

John R. Foster
Utah Field House of Natural History State Park Museum
435.789.3799
eutretauranosuchus@gmail.com

Steven Schamel
GeoX Consulting, Inc.
801.583-1146
geox-slc@comcast.net

Production

Cover Design and Desktop Publishing
Douglas A. Sprinkel

Cover

East view of the prominent 5.5-m-thick tuff bed at the base of the Lapoint Member of the Duchesne River Formation. The base of the light-colored tuff bed is used as the contact with the underlying Dry Gulch Creek Member of the Duchesne River Formation. This outcrop of the tuff is located about 13 km west of Vernal, Utah, just off Utah SR-121 at 40.416519 N. latitude and 109.746494 W. longitude. See figure 3 and appendix 1 in this article for details.

UGA Board

2020 President	Leslie Heppler	lheppler@utah.gov	801.538.5257
2020 President-Elect	Riley Brinkerhoff	riley.brinkerhoff@gmail.com	406.839.1375
2020 Program Chair	Paul Inkenbrandt	paulinkenbrandt@utah.gov	801.537.3361
2020 Treasurer	Greg Gavin	greg@loughlinwater.com	801.538.4779
2020 Secretary	Elliot Jagniecki	ejagniecki@utah.gov	801.537.3370
2020 Past President	Peter Nielsen	peternielsen@utah.gov	801.537.3359

UGA Committees

Environmental Affairs	Craig Eaton	eaton@ihi-env.com	801.633.9396
Geologic Road Sign	Greg Gavin	greg@loughlinwater.com	801.541.6258
Historian	Paul Anderson	paul@pbageo.com	801.364.6613
Membership	Rick Ford	rford@weber.edu	801.626.6942
Outreach	Greg Nielsen	gnielsen@weber.edu	801.626.6394
Public Education	Zach Anderson	zanderson@utah.gov	801.537.3300
	Matt Affolter	gfl247@yahoo.com	
Publications	Paul Inkenbrandt	paulinkenbrandt@utah.gov	801.537.3361
Publicity	Paul Inkenbrandt	paulinkenbrandt@utah.gov	801.537.3361
Social/Recreation	Roger Bon	rogerbon@xmission.com	801.942.0533

AAPG House of Delegates

2017–2020 Term	Tom Chidsey	tomchidsey@utah.gov	801.537.3364

State Mapping Advisory Committee

UGA Representative	Bill Loughlin	bill@loughlinwater.com	435.649.4005

Earthquake Safety Committee

Chair	Grant Willis	gwillis@utah.gov	801.537.3355

UGA Website — www.utahgeology.org

Webmaster	Paul Inkenbrandt	paulinkenbrandt@utah.gov	801.537.3361

UGA Newsletter

Newsletter Editor	Bill Lund	uga.newsletter@gmail.com	435.590.1338

Become a member of the UGA to help support the work of the Association and receive notices for monthly meetings, annual field conferences, and new publications. Annual membership is $20 and annual student membership is only $5. Visit the UGA website at www.utahgeology.org for information and membership application.

The UGA board is elected annually by a voting process through UGA members. However, the UGA is a volunteer-driven organization, and we welcome your voluntary service. If you would like to participate please contact the current president or committee member corresponding with the area in which you would like to volunteer.

Utah Geological Association formed in 1970 from a merger of the Utah Geological Society, founded in 1946, and the Intermountain Association of Geologists, founded in 1949. Affiliated with the American Association of Petroleum Geologists.

GEOLOGY OF THE INTERMOUNTAIN WEST
an open-access journal of the Utah Geological Association
Volume 7 *2020*

Fallout Tuffs in the Eocene Duchesne River Formation, Northeastern Utah—Ages, Compositions, and Likely Source

Michael S. Jensen[1], Bart J. Kowallis[1], Eric H Christiansen[1], Casey Webb[1], Michael J. Dorais[1], Douglas A. Sprinkel[2], and Brian Jicha[3]

[1] Department of Geological Sciences, Brigham Young University, Provo, UT, 84602; wasabae@gmail.com
[2] Azteca Geosolutions, Pleasant View, UT 84414; Utah Geological Survey, Salt Lake City, UT 84114; dsprinkel@gmail.com
[3] University of Wisconsin, Department of Geoscience, Madison, WI, 53706; bjicha@geology.wisc.edu

ABSTRACT

Thin fallout tuffs are common in the terrestrial deposits of the Eocene Duchesne River Formation on the flanks of the Uinta Mountains of eastern Utah. Their ages and compositions provide new insight into the tectonic events and magmatic history of the western Cordillera and provide important constraints on the Cenozoic land mammal chronology. Whole-rock compositions of the volcanic ash show that they underwent post-emplacement argillic alteration, typical of a wetland/floodplain depositional setting. However, immobile element ratios and abundances, such as Zr/Ti, La/Nb, and Y are typical of rhyolites formed in a subduction-related setting. Glass shards preserved in one sample all had SiO_2 values >75%, typical of high-silica rhyolite. Preserved phenocrysts in the ash beds include quartz, sanidine, plagioclase, and biotite with variable amounts of accessory zircon, apatite, titanite, and allanite. Biotite compositions have Fe/(Fe+Mg) ratios typical of calc-alkaline igneous rocks and clusters of chemical compositions suggest a genetic relationship to three or four separate eruptions. Sanidine compositions from five samples range from Or_{73} and Or_{79}. Only one sample had preserved plagioclase with compositions ranging between An_{22} – An_{49}. Allanite from the ash beds has lower total rare earth elements (REE) concentrations than allanite from other well-studied rhyolites. Titanite in one sample has lower concentrations of REE, Fe, and Al than expected of rhyolites and is probably detrital.

Plagioclase and sanidine from two different tuff beds near the middle of the Duchesne River Formation yielded analytically indistinguishable $^{40}Ar/^{39}Ar$ ages of 39.47 ± 0.16 Ma and 39.36 ± 0.15 Ma, respectively. These dates, along with the compositional data seem to limit the eruptive source for these fallout tuffs to the northeast Nevada volcanic field, one of the few volcanically active regions of western North America at the time.

These new radiometric ages, along with stratigraphic relations and previously published ages for tuffs in the Bishop Conglomerate (which unconformably overlies the Duchesne River Formation), constrain the timing of late Laramide uplift in the region from 39 to about 37 Ma and post-Laramide epeirogenic uplift from 34 Ma to 30 Ma. Finally, the ages also provide additional evidence that the Duchesnean North American Land Mammal Age ended in the Eocene, which was originally named and defined from the Duchesne River Formation.

Citation for this article.
Jensen, M.S., Kowallis, B.J., Christiansen, E.H, Webb, C., Dorais, M.J., Sprinkel, D.A., and Jicha, B., 2020, Fallout tuffs in the Eocene Duchesne River Formation, northeastern Utah—ages, compositions, and likely source: Geology of the Intermountain West, v. 7, p. 1–27, 2 appendices, supplemental data, https://doi.org/10.31711/giw.v7.pp1–27.

INTRODUCTION

Preserved volcanic ash in sedimentary rock sections can provide insights into the geologic history of a region through radioisotopic dating and geochemical analysis, leading to better interpretations of tectonic events and settings (Kowallis and others, 2001; Hildreth and Wilson, 2007; Smith and others, 2014; Christiansen and others, 2015; Hong and others, 2019). Radiometric dating of tuffs also provides better age constraints on sedimentary rocks and fossils (Kowallis and others, 1991, 1998, 2001; Riggs and others, 2003; Smith and Carrol, 2015). Additionally, accurate dates of volcanic ash in sedimentary succession can be used as important markers for stratigraphic correlation (Huff, 2016).

We have employed high-precision, single-crystal, $^{40}Ar/^{39}Ar$ laser-fusion dating along with whole-rock and mineral geochemical analyses on the fallout tuffs in the Duchesne River Formation located in the Uinta Basin of eastern Utah. Previous work on the Duchesne River Formation tuff beds has provided some information on their age (Andersen and Picard, 1974; Bryant and others, 1989; Sprinkel, 2007) but the dates were imprecise and geochemical data was essentially nonexistent. In the overlying Bishop Conglomerate, which also contains altered fallout tuffs, previous work has shown that more accurate and precise $^{40}Ar/^{39}Ar$ dating techniques and detailed chemical compositions can be used to constrain the timing, tectonic setting, and sources of altered middle Cenozoic tuffs, as well as inferences about the original composition (Kowallis and others, 2005). In this study, we attempt to answer the following questions:

1. What are the ages of the fallout tuffs within the Duchesne River Formation?
2. What phenoclasts are preserved within these tuffs and what are their compositions?
3. How has alteration affected the chemistry of the Duchesne River Formation tuffs and can inferences be made about their original composition?
4. Where is/are the eruptive source or sources of the tuffs?
5. Do more precise ages help to better constrain the age of fauna within the Duchesne River Formation, which serves as the type formation for the Duchesnean North American Land Mammal Age (NALMA)?
6. Do the ages obtained from the ash beds help constrain periods of uplift of the Uinta Mountains?

GEOLOGIC SETTING

Laramide Orogeny

The Laramide orogeny was characterized by basement block uplift along high-angle reverse faults apparently due to shallow subduction of the Farallon plate from 70-34 Ma (Dickinson and others, 1988; Liu and others, 2010; Jones and others, 2011; Fan and Carrapa, 2014; Yonkee and Weil, 2015). The east-west-trending Uinta Mountain range is one such basement block and has experienced multiple periods of uplift and erosion (Hamilton, 1978; Hansen, 1986; Dickinson and others, 1988) as recorded by the sediments in the adjacent Uinta Basin (figure 1), including the Green River, Uinta, and the Duchesne River Formations. Ponded basins, such as the Uinta Basin, were common during the Laramide and were often filled with fresh or saline lakes that acted as efficient sediment traps (Carroll and Bohacs, 1999; Tanavsuu-Milkeviciene and others, 2017). The lakes and fluvial environments were also efficient traps for erupted volcanic material, and fallout tuffs have been found in many of the formations throughout the strata within the Uinta Basin and have been used to date the timing of volcanic, tectonic, and sedimentary events (Bryant and others, 1989; Remy, 1992; Smith and others, 2003; Kowallis and others, 2005; Smith and Carroll, 2015).

During the early stages of the Laramide orogeny, volcanism was uncommon due to shallow subduction of the Farallon plate (DeCelles, 1994; Dickinson, 2004; Schellart and others, 2007). However, as the Farallon plate steepened, subduction-related volcanism resumed about 54 Ma beginning in present-day Montana and Idaho (Norman and Mertzman, 1991) and then migrated south into the Nevada-Utah region around 40 Ma, finally reaching the southern Great Basin about 36 Ma (Lipman and others, 1972; Humphreys, 1995; Castor and others, 2000, 2003; Best and others, 2013a). Volca-

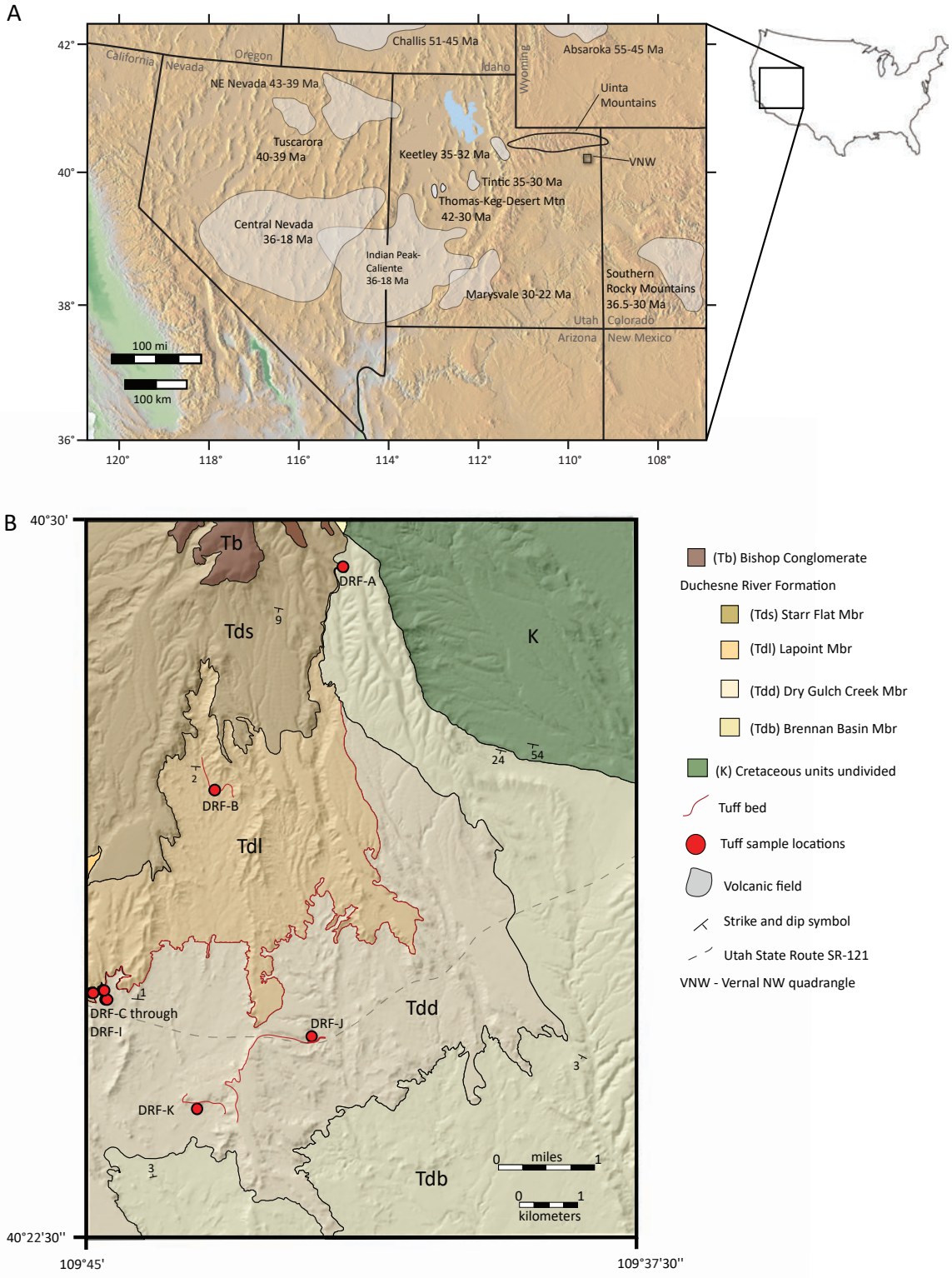

Figure 1. (A) Regional map of western United States with boundaries and ages of middle Cenozoic volcanic fields that formed as a result of slab rollback. (B) A simplified geologic map of the Vernal NW quadrangle showing locations of tuff samples, the principal geologic units, and contacts of the different members of the Duchesne River Formation. The Cretaceous units are undivided.

nic activity during this time period was so intense it has been called the middle Cenozoic ignimbrite flare-up. The Challis, Absaroka, northern Nevada-Utah, and the central and southern Great Basin volcanic fields document this time of intense volcanic activity (Brooks, 1995a; Chandler, 2006; Henry, 2008; Best and others, 2016). These repeated volcanic episodes have been proposed as a contributor to the global cooling at the Eocene-Oligocene boundary (Zanazzi and others, 2007; Jicha and others, 2009). Silicic volcanic rocks from this time period typically range from dacite to rhyolite in composition and are commonly preserved as fallout tuffs, ash-flow tuffs, flow breccias, and silicic domes (Lipman and others, 1972; Brooks and others, 1995c). Like other distal fallout tuffs, the Duchesne River Formation tuffs were likely sourced from large plinian or coignimbrite eruptions (Blaylock, 1998; Kowallis and others, 2005; Chandler, 2006; Christiansen and others, 2015).

Duchesne River Formation Stratigraphy

Sedimentary rocks, which record the uplift and erosion history of the Uinta Mountains and contain fallout tuffs that can be used to study and date that record, are well exposed on the southern flanks of the Uinta Mountains in the Vernal NW quadrangle just west of Vernal, Utah (figure 1). Along with Cretaceous units, the predominant formation within the quadrangle is the Duchesne River Formation where all four members (in ascending stratigraphic order: Brennan Basin, Dry Gulch Creek, Lapoint, and Starr Flat) are exposed (figure 2). Tuffaceous beds were not found in the basal Brennan Basin Member and the capping Starr Flat Member in the study area; however, tuff beds have been reported within these members elsewhere in the Uinta Basin region (Sprinkel, 2007, 2018a). The Dry Gulch Creek and Lapoint Members contain numerous tuffaceous beds. These members are predominantly composed of siltstone and mudstone that intertongue with fine- to medium-grained sandstone and conglomerate with both members becoming progressively coarser towards the uplifted Uinta Mountain front (Warner, 1966; Andersen and Picard, 1972, 1974; Sato and Chan, 2015; Webb, 2017). Tuff beds in the Dry Gulch Creek and Lapoint Members have been mostly altered to clay minerals (Andersen and Picard, 1974). They are light to medium gray and stand out against the moderate-red to reddish-brown siltstone and mudstone (figure 3). Several tuff beds are laterally extensive throughout much of the quadrangle and the lowermost tuff bed is used as the contact between the Lapoint and Dry Gulch Creek Members (Webb, 2017) (figure 3a).

The oldest and youngest members of the Duchesne River Formation, the basal Brennan Basin Member and the capping Starr Flat Member, respectively, are predominantly pebble to boulder conglomerates with minor sandstone and siltstone, indicating they either were deposited in closer proximity to the uplifting Uinta Mountain front to the north or were deposited when streams flowing off the uplift were transporting coarse material farther out into the basin as a result of increased gradient (Sato and Chan, 2015). The Starr Flat Member is capped by the Gilbert Peak erosion surface, a widespread Oligocene surface of erosion and non-deposition found on both the south and north flanks of the Uinta uplift (Hansen, 1986; Sprinkel, 2007; Webb, 2017). The Gilbert Peak erosion surface is considered to mark the end of the Laramide orogeny in the Uinta Basin region (Hansen, 1986; Aslan and others, 2017). The stratigraphy and distribution of the Duchesne River Formation members within the study area are reported in greater detail in Webb (2017).

In addition to the tuff beds, the Duchesne River Formation also contains key mammal fossils and has been used as the type section of the Duchesnean NALMA (Wood and others, 1941; Clark and others, 1967; Prothero, 1995). The Duchesnean NALMA is used throughout North America and the fauna within that time period are used to better understand the evolution of animals and climate in North America during the middle Eocene (Emry, 1981; Rassmussen and others, 1999; Alroy, 2000).

SAMPLING AND ANALYTICAL METHODS

Stratigraphic relations and structural evolution of the area were established by geological mapping (Webb, 2017). During the course of the mapping, four samples were collected from three tuff beds within the upper and

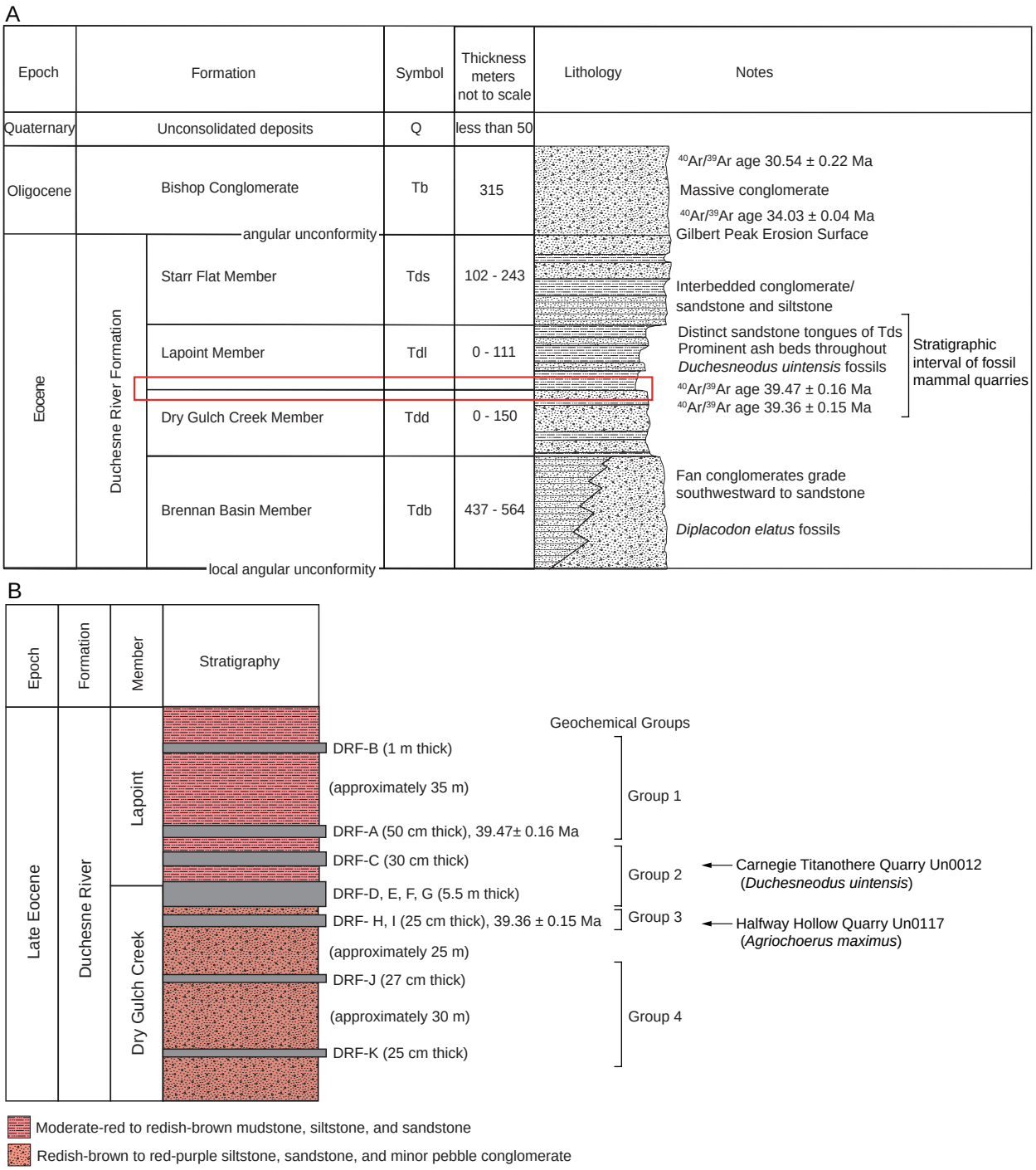

Figure 2. (A) Stratigraphic column of Paleogene units in the Vernal NW quadrangle from Webb (2017). $^{40}Ar/^{39}Ar$ ages from the Bishop Conglomerate are from Kowallis and others (2005) and fossils are from Burger and Tacket (2014). Red box indicates area of stratigraphic column shown in part B. (B) Stratigraphic column of the Dry Gulch Creek and Lapoint Members of the Duchesne River Formation showing the relative locations and thicknesses of the tuff beds (gray). Note that samples DRF-D, DRF-E, and DRF-F are from the same 5.5-m-thick tuffaceous bed which serves as the contact between the Dry Gulch Creek and Lapoint Members. Samples DRF-H and DRF-I are also from the same tuffaceous bed but collected from different locations about 2 km apart. Geochemical groups based on the chemical composition of the samples within each tuff. Note that the tuffs are grouped stratigraphically.

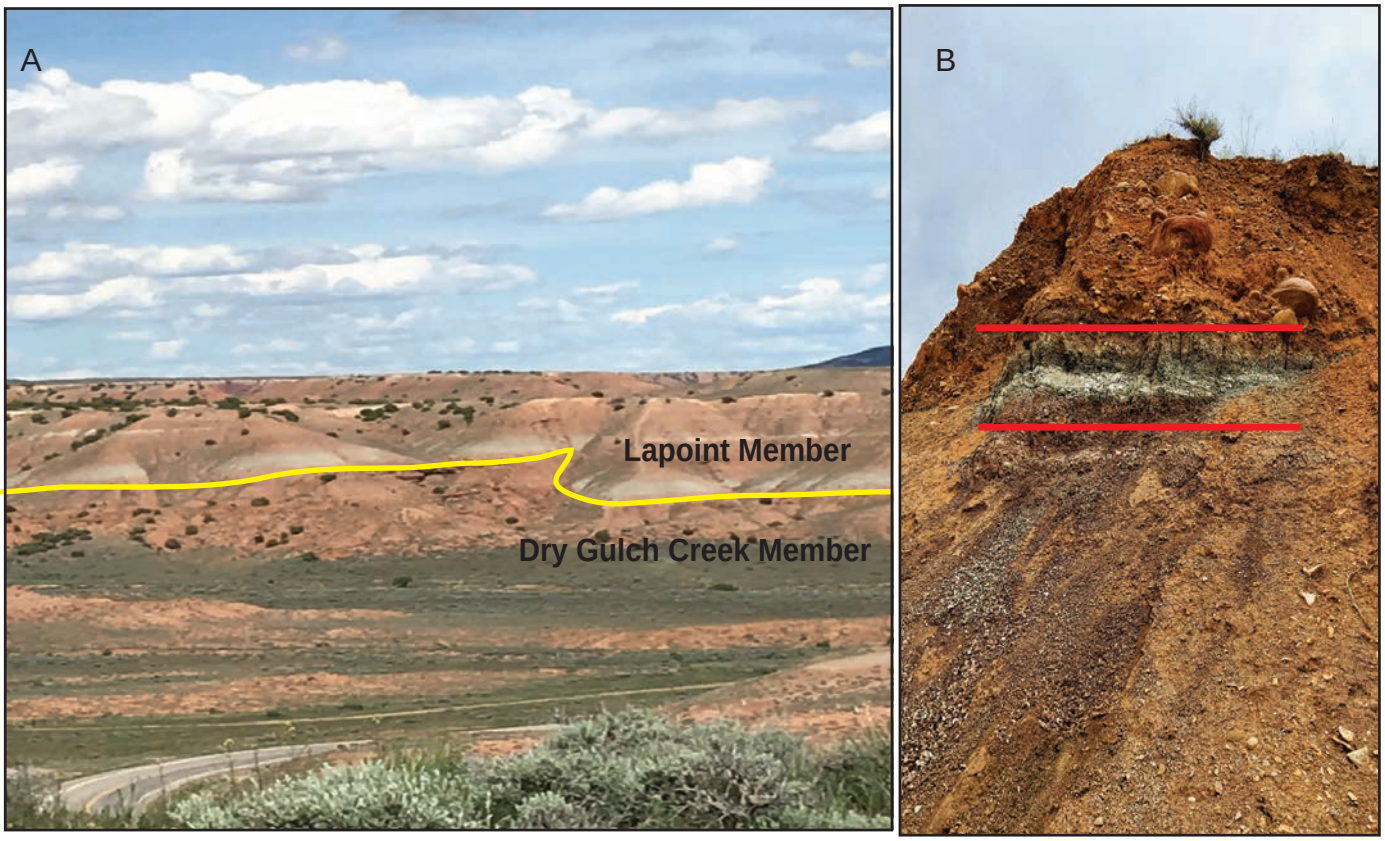

Figure 3. (A) View to the east of the basal 5.5-m-thick tuff bed at the contact (underlined in yellow) between with Dry Gulch Creek and the Lapoint Members. The gray color of the ash stands out against the reddish-orange colors of the siltstone. Samples DRF-D, DRF-E, DRF-F, and DRF-G were collected from this key layer which shows evidence of detrital mixing and has likely been thickened by post-sedimentary processes. (B) Collection site of sample DRF-C shown between the red lines is 18 m above the basal ash bed in A, which is covered by Quaternary unconsolidated gravel.

middle Dry Gulch Creek Member and seven samples were collected from four tuff beds within the Lapoint Member and within the Vernal NW quadrangle (table 1). Roughly 5 to 8 kg of sample was collected at each site (site descriptions and photographs can be found in appendix 1). A split of each sample was processed to liberate the mineral phenoclasts, which were extracted by standard washing and heavy liquid techniques. Phenocrysts were mounted in epoxy and then polished for microprobe analysis at Brigham Young University (BYU). Table 2 summarizes the analytical parameters used for each mineral. A portion of each sample was also prepared for X-ray fluorescence (XRF) analyses of major and trace elements also at BYU.

Two hundred sanidine grains from sample DRF-H and two hundred plagioclase grains from DRF-A were hand-picked from the clean concentrates at BYU. They were dated using single crystal $^{40}Ar/^{39}Ar$ laser fusion methods at the University of Wisconsin-Madison WiscAr Geochronology Lab. The $^{40}Ar/^{39}Ar$ ages were calculated relative to the FC-201 sanidine standard age of 28.201 Ma and a total ^{40}K decay constant of 5.643 e-10/a (Kuiper and others, 2008). Methodology for laser fusion dating of single crystals of sanidine are outlined on the WiscAr Lab website (http://geochronology.geoscience.wisc.edu/analytical-approaches/). A summary of all the ages and the analytical parameters is given in appendix 2. One of the benefits of the single crystal method is that anomalously old or young grains can be identified and removed from a weighted average and a more accurate

Table 1. Characteristics of tuffs from the Duchesne River Formation.

Member	Sample	Latitude	Longitude	Phenocryst Assemblage	Age (Ma)	Temperature (°C)		Rock Type (Zr/Ti -Nb/Y)	Tectonic Settting (Nb-Y)
						Feld	Bt		
Lapoint	DRF-A	40.491478	-109.746676	Qz-Bt-Sa-Pl-Aln-gls-Zrn	39.47 +/- 0.16	630	711	Dacite	Volcanic Arc
Lapoint	DRF-B	40.449856	-109.720892	Qz-Bt-Sa-Mc			704	Dacite	Volcanic Arc
Lapoint	DRF-C	40.417679	-109.749658	Qz-Bt-Aln			658	Dacite	Volcanic Arc
Lapoint	DRF-D	40.416545	-109.746362	Qz-Bt-Ap-Zrn			697	Dacite	Volcanic Arc
Lapoint	DRF-E	40.416564	-109.746445	Qz-Bt				Dacite	Volcanic Arc
Lapoint	DRF-F	40.416583	-109.746469	Qz-Bt			645	Dacite	Volcanic Arc
Lapoint	DRF-G	40.416519	-109.746494	Qz-Bt-Mc			650	Dacite	Volcanic Arc
Dry Gulch Creek	DRF-H	40.418116	-109.747051	Qz-Bt-Sa-Mc-Aln			638	Trachyte	Volcanic Arc
Dry Gulch Creek	DRF-I	40.418127	-109.747087	Qz-Bt-Sa-Mc-Aln-Ttn-Zrn	39.36 +/- 0.15		645	Trachyte	Volcanic Arc
Dry Gulch Creek	DRF-J	40.409754	-109.699966	Qz-Bt-Sa			698	Rhyolite	Volcanic Arc
Dry Gulch Creek	DRF-K	40.397333	-109.726184	Qz-Bt-Mc			696	Rhyolite	Volcanic Arc

Note: Feldspar temperature calculated using the thermodynamic parameters of Elkins and Grove (1990) at a pressure of 5 kb. Biotite temperatures are an average of multiple grains, calculated using the thermometer of Luhr and others (1984). Mineral abbreviations from Whitney and Evans (2010). Aln is allanite, Ap is apatite, Bt is biotite, gls is glass, Mc is microcline, Pl is plagioclase, Sa is sanidine, Ttn is titanite, Qz, is quartz, Zrn is zircon.

eruption age can be determined. This method is particularly critical for tuff beds collected from sedimentary sections where even slight reworking of the ash can contaminate it. Both samples contained detrital feldspar much older than the Duchesne River Formation. One of the drawbacks of single crystal analysis, however, is that because the crystals and argon signal sizes are small, the analytical uncertainties are higher than they would be using the multi-crystal fusion method; consequently, the analytical errors are on the order of 100,000 years rather than 10,000 years.

ISOTOPIC AGES

Several isotopic ages have previously been reported from the prominent tuff bed near the base of the Lapoint Member of the Duchesne River Formation (table 3). Fairly consistent K-Ar and $^{40}Ar/^{39}Ar$ biotite ages of approximately 41 ± 0.5 Ma from this bed have been reported by McDowell and others (1973), Andersen and Picard (1974), and Prothero and Swisher (1992) whereas fission track ages from the same bed in the Lapoint Member averaged 34 ± 1–3 Ma (Bryant and others, 1989). Additionally, a biotite K-Ar age of 37.6 ± 1.4 Ma and a zircon fission track age of 36.7 Ma ± 3.9 Ma were obtained from a tuff within the younger Starr Flat Member from the Neola NW quadrangle (table 3). The previous K-Ar and fission track ages from the Duchesne River Formation all have relatively large uncertainties. The biotite ages may also suffer from alteration, typical of biotite in this type of environment, giving erroneous ages (Smith and others, 2008). We chose to date feldspar because it is more resistant than biotite to alteration and

Table 2. Parameters for electron-microprobe analyses.

Mineral	Standard	Analytical conditions for unknown
Biotite	Lemhi Biotite	20 nA current, 15kv acceleration voltage, 5µ beam size
Sanidine	orthoclase	20 nA current, 15kv acceleration voltage, 5µ beam size
Plagioclase	anorthosite	20 nA current, 15kv acceleration voltage, 5µ beam size
Allanite	none	20 nA current, 15kv acceleration voltage, 5µ beam size
Titanite	Sphene-T	30 nA current, 15kv acceleration voltage, 10µ beam size
Apatite	Apa-Durango	10 nA current, 15kv acceleration voltage, 5µ beam size
Glass	Rhyo-Gls	10 nA current, 15kv acceleration voltage, 5µ beam size

Note: Names of standards are from the list of standards used by the BYU Department of Geological Science.

Table 3. Compilation of selected isotopic ages of the Duchesne River Formation.

Reference/Report	Sample ID	Age ±2sd (Ma)	Method	Member	7.5' Quadrangle	Latitude (N)	Longitude (W)
This Study	DRF-H	39.36 ± 0.15	$^{40}Ar/^{39}Ar$, plagioclase	Lapoint	Vernal NW	40° 24'59.4"	109° 44'47.6"
This Study	DRF-A	39.47 ± 0.16	$^{40}Ar/^{39}Ar$, sanidine	Dry Gulch Creek	Vernal NW	40° 29'28.9"	109° 41'28.94"
Bryant and others (1989)	N-83-2	36.7 ± 3.9	Fission Track, zircon	Starr Flat	Neola	40° 28'43"	110° 05'54'
Bryant and others (1989)	ICP-1A	30.5 ± 1.4	Fission Track, zircon	Starr Flat	Ice Cave Peak	40° 35'49"	109° 59'52"
Constenius and others (2011)	KNC070109-1	38.90 ± 0.80	U-Pb, zircon	Starr Flat	Wolf Creek Summit	40° 23'240"	111° 00'908"
Bryant and others (1989)	VNW-1	36.9 ± 1.8	Fission Track, zircon	Lapoint	Vernal NW	40° 24'33"	109° 42'01"
Bryant and others (1989)	LA-1	35.2 ± 1.6	Fission Track, zircon	Lapoint	Lapoint	40° 24'52"	109° 45'43"
Prothero and Swisher (1992)	LP1	39.47 ± 0.17	$^{40}Ar/^{39}Ar$ biotite	Lapoint	Vernal NW	Not reported	Not reported
Bryant and others (1989)	BLU-83-1	33.0 ± 3.4	Fission Track, zircon	Dry Gulch Creek	Bluebell	40° 19'41"	110° 09'17"
Bryant and others (1989)	BLU-83-2	34.5 ± 4.4	Fission Track, zircon	Dry Gulch Creek	Bluebell	40° 19'40"	110° 09'21"
UGS Apatite to Zircon (2014)	HC08122012-1	40.66 ± 1.88	U-Pb, zircon	Brennan Basin	Hancock Cove	40° 18'02.89"	110° 04'58.03"

typically provides more accurate ages (Kowallis and others, 1998, 2001, 2005).

Sanidine extracted from our sample DRF-H gave a $^{40}Ar/^{39}Ar$ age of 39.36 ± 0.15 Ma and plagioclase from DRF-A gave an age of 39.47 ± 0.16 Ma (figure 4). DRF-H was taken from a tuff bed at the top of the Dry Gulch Creek Member, only 2 to 3 m from the contact with the Lapoint Member. DRF-A was taken from a tuff bed within the overlying Lapoint Member several kilometers northeast of DRF-H near where the Lapoint Member pinches out between the Starr Flat Member and Brennan Basin Member (figure 1). The ages are stratigraphically inverted but are not analytically distinguishable from one another. Despite being very close in age, DRF-A and DRF-H are not from the same ash bed based on field mapping and chemical and mineralogical differences outlined below. This is significant because sample DRF-A represents a tuff bed that was mapped as part of the Starr Flat Member (Sprinkel, 2007). Our recent mapping at 1:24,000 scale (Webb, 2017) and the new age suggest that the tuff bed is from the upper part of the Lapoint Member where the Lapoint and Starr Flat Members intertongue. The analytical uncertainties for these new ages are much smaller than previous ones and constrain the boundary between the Lapoint and Dry Gulch Creek Members to about 39.4 Ma. These ages are significantly younger than the previously reported ~41 Ma ages from the same series of tuff beds (McDowell and others, 1973; Andersen and Picard, 1974; Prothero and Swisher, 1992).

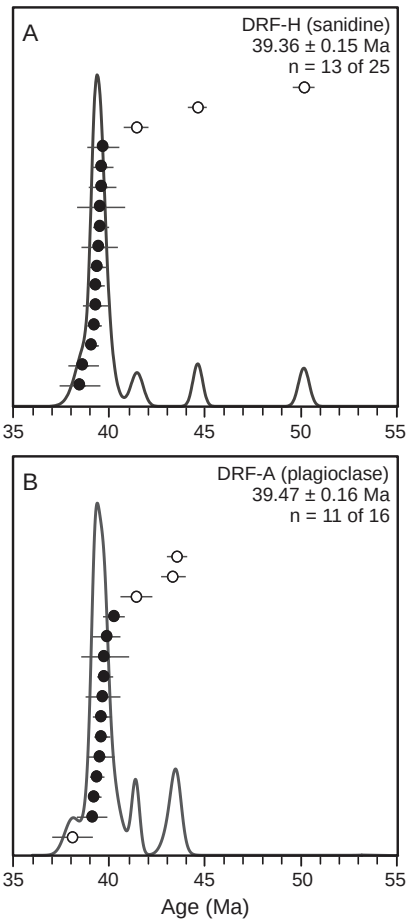

Figure 4. Rank order plots with probability density curves for feldspar ages from samples DRF-H (A) and DRF-A (B) from the Dry Gulch Creek and Lapoint Members of the Duchesne River Formation, respectively. Individual $^{40}Ar/^{39}Ar$ dates, as well as weighted mean ages, are shown with 2σ analytical uncertainties. Filled circles are the ages that were used in the age calculation.

MINERAL ASSEMBLAGES AND COMPOSITIONS

In addition to providing ages, magmatic phenocrysts in tuff beds can provide information that can help in determining the composition of the source magma, in correlating ash beds across a broader area, and provide insights into the tectonic setting. Table 1 summarizes the mineral assemblage of each of the samples collected from the Duchesne River Formation. The presence of quartz, biotite, and sanidine and absence of pyroxene and hornblende is a common subduction-related rhyolitic mineral assemblage and typical of other volcanic ash beds from the late Eocene of western North America (Lipman and others, 1972). Allanite was found in four samples. Titanite and apatite were the least abundant minerals and were only found in one sample each. Because these ashes were deposited in a dominantly fluvial environment, there is an inherent risk of contamination by detrital grains and all samples contained sedimentary grains of quartz, carbonate, and diagenetic clay.

Quartz

Quartz grains were present in all the Duchesne River Formation samples. Igneous quartz grains were identified by their prismatic, euhedral shape, and presence of glassy melt inclusions. Detrital quartz grains were rounded, frosted, lacked melt inclusions, and tended to be larger than the volcanic quartz grains.

Biotite

Biotite phenocrysts were present in all the Duchesne River Formation tuffs and are the main mafic phase present. In several samples, abundant biotite was visible in the field without the aid of a hand lens. In general, biotite is less resistant to the effects of weathering than sanidine, quartz, and allanite. The biotite phenocrysts collected showed signs of alteration with many grains being rounded and light brown in color; however, no evidence of chloritic alteration was found in the polished grain mounts. Chloritic alteration is a concern because K can be replaced with H_2O and Cl during diagenesis (Bisdom and others, 1982; Smith and others, 2008). These chemical changes lead to low analytical totals and the resulting isotopic ages cannot be considered accurate (Smith and others, 2008). To avoid alteration, only black, euhedral grains were picked for electron microprobe analysis and from those, only analyses with totals (not including water) of 90% or above were considered.

Al, Fe, and Mg in biotite are typically fairly immobile and may help in understanding the original composition of the tuff beds (Christiansen and others, 2015). Molar Fe/(Fe+Mg) and total Al (atoms per formula unit – apfu) plot within or near the calc-alkaline rhyolite field (figure 5) and are similar to biotites from the subduction-related Oligocene Fish Canyon Tuff and Jurassic tuffs from the Temple Cap, Carmel, and Morrison Formations (Kowallis and others, 2001; Christiansen and others, 2015). Total Al plots between 1.2 and 1.5 apfu for biotite in seven of the samples, but biotite in DRF-C, DRF-D, DRF-F, and DRF-G have total Al greater than 1.5 apfu. Samples DRF-D, DRF-F, and DRF-G are from different horizons within the same prominent ash bed at

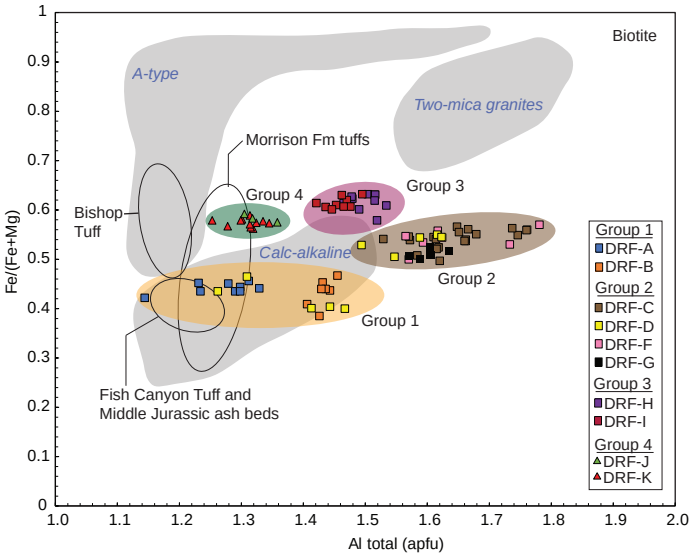

Figure 5. Compositions of biotite from the tuffs of the Duchesne River Formation compared to the Bishop Tuff, Fish Canyon Tuff, Morrison Formation tuffs, and Middle Jurassic tuffs from the Carmel and Temple Cap Formations, which are all subduction-related pyroclastic deposits. Fields for different types of granite are from Christiansen and others (1986). The four clusters formed by the Duchense River Formation samples are grouped stratigraphically. Compositions are presented in atoms per formula unit (apfu).

the same geographic location at the base of the Lapoint Member (figures 1 and 2, appendix 1) and form the high Al group. An enrichment of Al is sometimes the result of alteration as the more mobile elements like K and Na are removed and Al becomes relatively enriched (Christiansen and others, 2015). However, the grains with high Al also have K levels of at least 8 wt.% (Jensen, 2017), an indication that the biotite has undergone little alteration. Sericitic alteration could explain the elevated Al paired with normal levels of K but sericitic alteration occurs at higher temperatures and also decreases Mg below a 3/2 Mg/Fe ratio, which is not the case for the Duchesne River Formation tuffs (figure 6). Additionally, these samples have relatively high analytical totals (93 > wt.%) compared to other Duchesne River Formation biotite phenocrysts. DRF-D, DRF-F, and DRF-G were collected from the top, middle, and bottom of the same thick ash bed at the same locality at the base of the Lapoint Member and they all have the Fe/Mg ratios, Al values, and high analytical totals described above; this consistency would not be expected if the biotite was altered by secondary processes. Consequently, we consider these biotites to have magmatic compositions.

The total Al vs Fe/(Mg+Fe) diagram also reveals distinct clusters of biotite from the Duchesne River Formation tuffs (figure 5). The clustering follows stratigraphic order with the oldest middle Dry Gulch Creek samples, DRF-K and DRF-J, plotting together. The upper Dry Gulch Creek samples DRF-H and DRF-I were taken from the same ash bed at two different localities about 2 km apart and form an isolated cluster. These two groups have Fe/(Mg+Fe) ratios slightly higher than typical biotite in calc-alkaline rhyolite, which could be an indication of a more evolved and differentiated melt or that crystallization occurred at a lower fO_2 than typical calc-alkaline rhyolites.

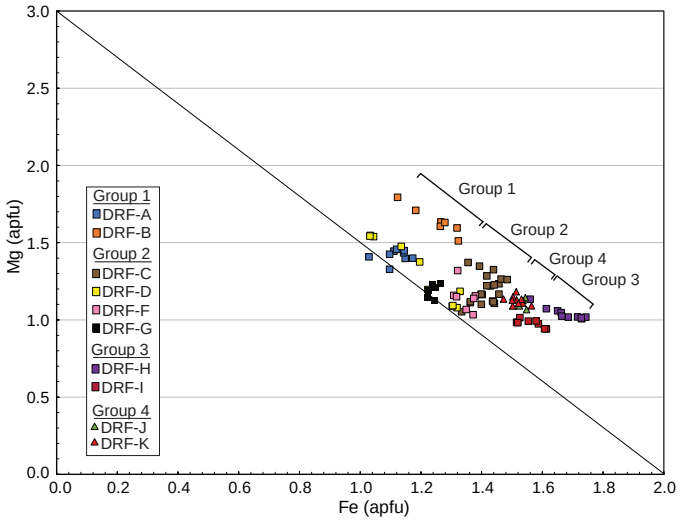

Figure 6. Mg and Fe abundances for biotite phenocrysts from the tuffs of the Duchesne River Formation plot near or above a ratio of 3 to 2. A 3/2 ratio eliminates sericite alteration as a cause for the high amounts of Al and K in these tuffs. The Mg/Fe ratio gradually increases over time.

Also seen on figure 5, five biotite grains from DRF-D (yellow) have lower total Al and Fe/(Fe+Mg) ratios than the rest of DRF-D grains. These grains have analytical totals above 96 wt.% so their anomalous compositions could be an indication of a detrital component or of the secondary mixing of ash from two separate eruptions rather than alteration. DRF-D was collected at the top of the prominent, basal ash bed of the Lapoint Member (figure 2 and appendix 1) and could have experienced reworking in the floodplain depositional environment. DRF-C represents a tuff bed about 10 m above the basal Lapoint Member ash bed and also lies in the high Al group. Finally, the middle Lapoint samples, DRF-B and DRF-A, form a loose cluster with similar Fe/(Fe+Mg) ratios within the range of typical calc-alkaline rhyolites

To see if the groups selected on figure 5 are statistically significant, a hierarchical cluster analysis was run using all the elements analyzed in biotite according to Ward's minimum variance method (Ward, 1963) using the JMP software. A constellation plot (figure 7) shows that the samples in the total Al diagram cluster in the same way when TiO_2, Al_2O_3, FeOt, MgO, Na_2O, K_2O, F, and Cl are all considered. These four clusters of biotite analyses are grouped stratigraphically which suggests that the composition of the magmatic source of the Duchesne River Formation tuffs became less evolved over time. For example, Fe drops from 1.8 to 1.0 apfu, while Mg increases from 1.0 to 1.7 apfu (figure 6) from the lower Dry Gulch Creek Member tuffs to the mid Lapoint Member tuffs.

Biotite compositions are also useful in geothermometry (Luhr and others, 1984). Titanium is a temperature-sensitive element in biotite and increases with increasing temperature (figure 8). Temperature calculations from the biotite minerals from the Duchesne River

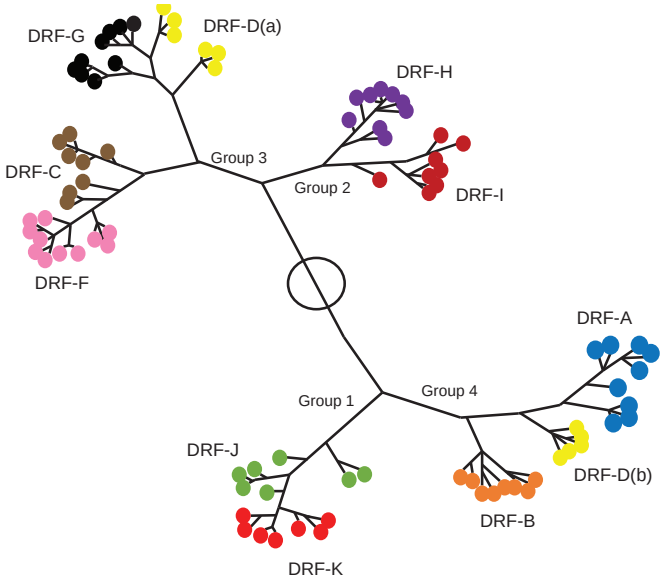

Figure 7. Constellation plot showing how individual biotite analyses compare to each other on the basis of oxide wt.% of TiO_2, Al_2O_3, FeOt, MgO, Na_2O, K_2O, F, and Cl. Note that DRF-D was separated into different clusters (a) and (b). This mixing is likely due to post-deposition detrital mixing. DRF-F, DRF-C, DRF-G, and DRF-D are somewhat mixed but become more distinctive when all elements are considered, especially SiO_2, FeOt, and MgO.

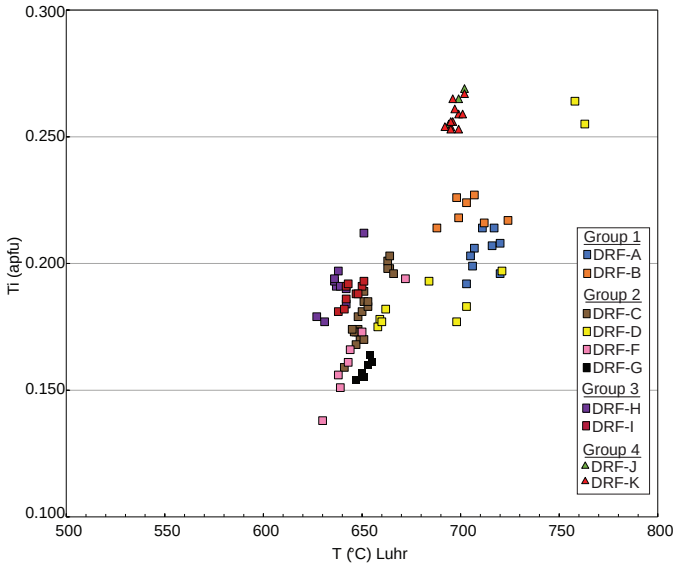

Figure 8. Temperatures calculated from biotite compositions using the thermometer of Luhr and others (1984) which depends on the Ti/Fe ratio. The groups in this diagram are the same as in figure 5.

Formation tuffs range between 625 and 725°C. The low end of the range is suspect because typical biotite temperatures in fresh rhyolite are close to 700°C but samples DRF-C through DRF-I all plot at 650°C or lower. These low-temperature biotite minerals also show enrichment of Al but maintain K abundances greater than 0.9 apfu. Speculatively, the low temperatures and the high Al and K content could be the result of metasediments being incorporated into the magma prior to eruption.

Comparison of $\log(X_{Mg}/X_{Fe})$ and $\log(X_F/X_{OH})$ from the Duchesne River Formation biotites (figure 9) plot in the oxidized, moderately contaminated (I-MC) field (Ague and Brimhall, 1988). The biotites have lower $\log(X_F/X_{OH})$ than that in the Oligocene Fish Canyon Tuff and only overlap the lower $\log(X_F/X_{OH})$ of biotite from the Late Jurassic Morrison Formation tuffs from eastern Utah (Christiansen and others, 2015). Based on lower Mg/Fe ratios, they are also more reduced than most of the Middle Jurassic ash beds of the Temple Cap and Carmel Formations collected in southwestern Utah (Kowallis and others, 2001). Nonetheless, they are similar to Sierran granites (Ague and Brimhall, 1988) and thus are similar to other subduction-related, typically oxidized silicic suites.

Feldspar

Alkali feldspar was the most common feldspar found in the Duchesne River Formation tuffs and was present in six samples whereas phenocrysts of plagioclase were found in only one sample (DRF-A from the middle part of the Lapoint Member). Plagioclase phenocrysts were commonly zoned and compositions ranged from An_{50} to An_{17} (figure 10). Since plagioclase has a low tolerance to weathering, it is unlikely to be a detrital component and is considered volcanic. Of the six samples with alkali feldspar, only four contained volcanic sanidine with Or_{72}-Or_{81}. The other alkali feldspar grains in DRF-B, DRF-G, DRF-I, and DRF-K are detrital with Or values $>Or_{89}$; in DRF-H these are likely the grains that give older Eocene to Jurassic ages and usually have higher K/Ca ratios.

Using plagioclase and sanidine from DRF-A, a two-feldspar eruption temperature was calculated using

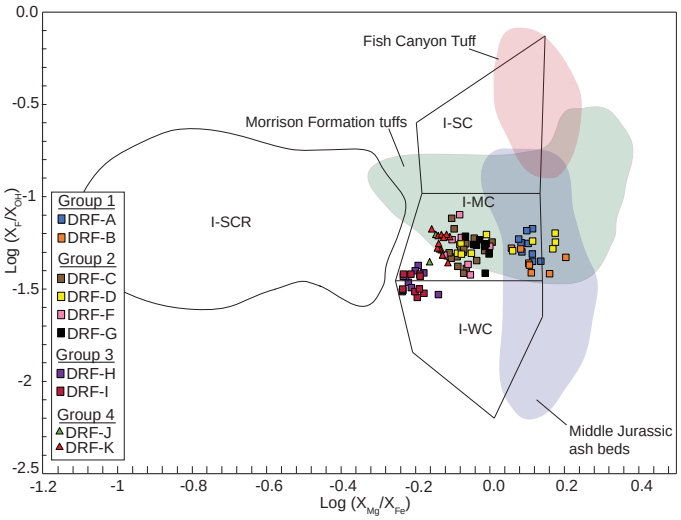

Figure 9. Compositions of Duchesne River Formation biotite phenocrysts compared to the Fish Canyon Tuff, Morrison Formation tuffs of Christiansen and others (2015), and to ash beds in the Middle Jurassic of southern Utah (Kowallis and others, 2001) in terms of $\log(X_{Mg}/X_{Fe})$ vs. $\log(X_F/X_{OH})$, where X is mole fraction. Granite fields are for Sierra Nevada granitoids from Ague and Brimhall (1988): I-SCR—I-type, strongly contaminated and reduced; I-SC—I-type, strongly contaminated; I-MC—I-type, moderately contaminated; I-WC—I-type, weakly contaminated. These biotites are most like those in the moderately contaminated granites.

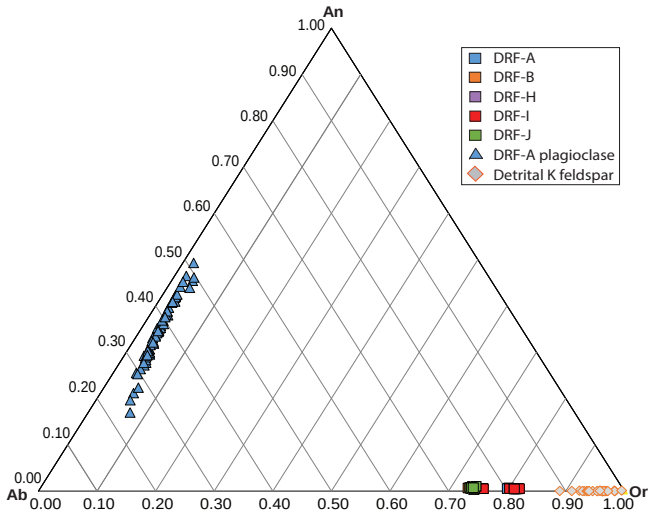

Figure 10. Ternary diagram of feldspar compositions. DRF-A is the only sample with two feldspars. Sanidine phenocrysts from DRF-I and -J have relatively high Or levels. Potassium feldspars with $>Or_{90}$ were interpreted to be detrital grains from plutonic rocks. These high Or grains are Late Jurassic to Early Cretaceous in age based on $^{40}Ar/^{39}Ar$ ages (Jensen, 2017).

SolvCalc (Wen and Nakvasil, 1994) and the thermodynamic parameters of Elkins and Grove (1990). Average temperatures of 643°C, 630°C, and 608°C were calculated at 5, 3, and 2 kilobars, respectively, using the average composition of the five most sodic plagioclase grains ranging from An_{20} to An_{27} and one Or_{79} sanidine grain. The temperatures are low compared to other volcanic rhyolite feldspars and since only one sanidine grain was used in the calculations these temperatures are not likely to be reliable.

Allanite

Allanite, a common accessory mineral in silicic igneous rocks, is a complex, rare earth element-rich mineral of the epidote group with a general formula of $A_2M_3Si_3O_{11}(O, F)(OH)$, in which A is commonly Ca^{2+}, Th^{4+}, REE^{3+}, or U^{4+}, and M typically includes Al^{3+}, Fe^{3+}, or Fe^{2+} (Deer and others, 1997). Rare earth elements (RRE) are essential constituents in allanite through the coupled substitution of $Ca^{2+} + Fe^{3+} = REE^{3+} + Fe^{2+}$ (Giere and Sorensen, 2004). Euhedral grains of allanite were found in three different tuff beds in the Duchesne River Formation, represented by four samples—DRF-A, DRF-C, DRF-H, and DRF-I. The grains are relatively unaltered with analytical totals between 98% and 100%.

Duchesne River Formation allanite minerals have CaO concentrations ranging from 11 to 13 wt.%, which is several percent higher than in allanite from the Toba and Bishop Tuffs of Sumatra and California, respectively (figure 11). They also have about 0.65 apfu total light rare earth elements (LREE), which is about 0.3 apfu less than the allanites in the Toba or the highly-evolved Bishop Tuff as shown on figure 12. High Ca and low REE could be an indication that the melt in which the allanite formed was slightly depleted in REE and so Ca remained high in the A site. Chesner and Ettlinger (1989), however, found that REE abundance in allanite may not be a good indicator of REE concentrations in the magmatic melt. For example, allanite from the Bishop Tuff (Hildreth, 1979) has higher REE concentrations than allanite in the Toba Tuff but lower whole-rock REE abundances. Chesner and Ettlinger (1989) conclud-

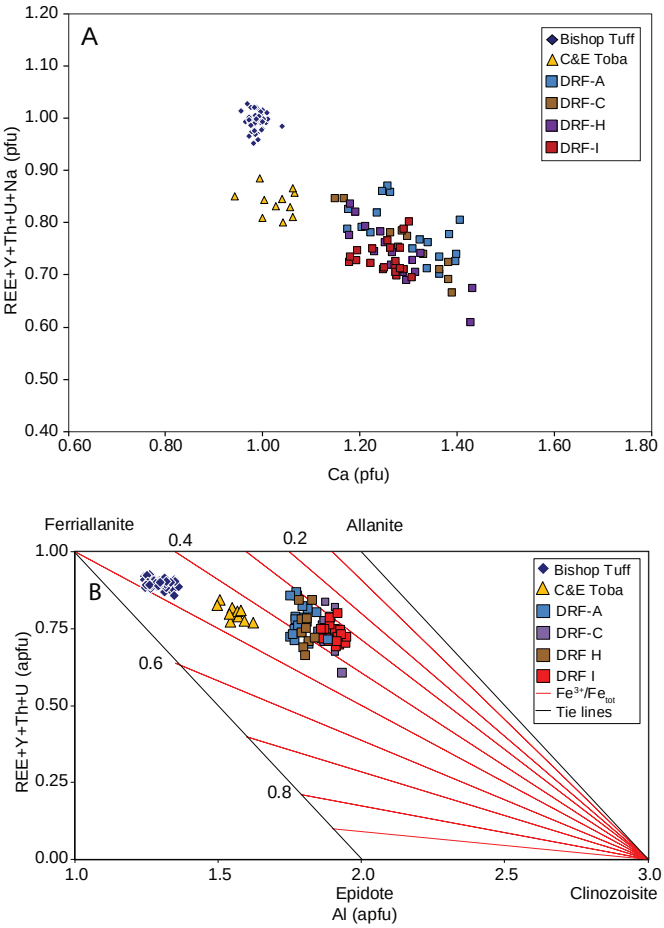

Figure 11. (A) Allanite phenocryst compositions from the Duchesne River Formation tuffs compared to allanite in the Bishop Tuff (California) and Toba Tuff (Sumatra), which are relatively more enriched in REEs and other A-site substitutions. (B) Duchesne River Formation allanites have lower inferred $Fe^{3}+/Fe_{Total}$ ratios (0.3–0.4) than both the Bishop and Toba Tuffs, implying lower fO_2 in the parent magmas.

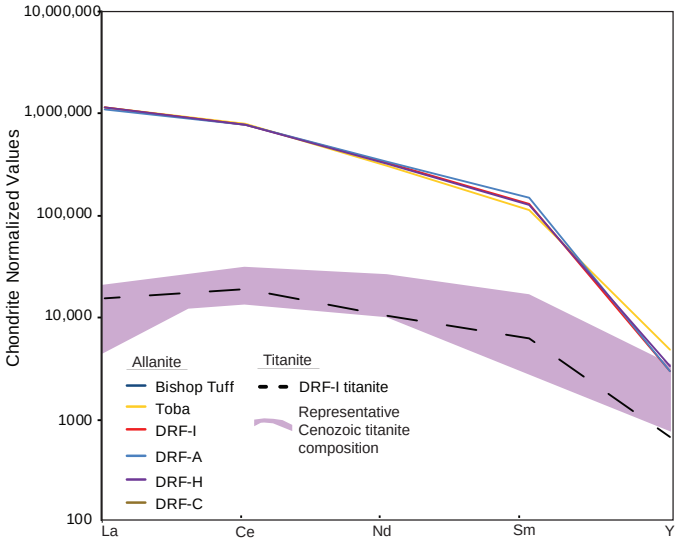

Figure 12. LREE-Y pattern for allanite in tuffs from the Duchesne River Formation compared to the average LREE abundances of allanite in the Bishop and Toba Tuffs; all are quite similar. The LREE-Y pattern for average titanite in sample DRF-I is plotted for comparison. Allanites are strongly enriched in LREEs, including Y, compared to titanites. The compositional field for titanite in other Cenozoic tuffs of the Great Basin is shown for comparison.

ed that physical parameters such as temperature exert a greater control on REE substitution in allanite than composition of the coexisting melt and suggested that higher temperatures correlate with higher REE abundances in allanite. The allanite-bearing tuffs from the Duchesne River Formation apparently had low eruptive temperatures around 650 to 710°C based on biotite compositions. The lower REE content of allanite thus seems to agree with this notion. Low eruption temperatures could explain other chemical differences between the Duchesne River Formation allanite and other well-studied tuffs, if Ti in the octahedral site is a function of temperature as it is in biotite and hornblende. Allanite in Duchesne River Formation tuffs has Ti concentrations between 0.0 to 0.06 apfu compared with 0.06 to 0.12 for allanite in the Toba Tuff and 0.16 and 0.19 for the Bishop Tuff.

Petrik and others (1995) argued that the REE and Al content of allanite is a function of Fe^{3+}/Fe_{Total} and is thus an indicator of magmatic fO_2. In this regard, allanite from Duchesne River Formation tuffs contains more Al than the other silicic tuffs used for comparison (>1.8 vs. 1.2–1.6 apfu). As a consequence, allanite has relatively low calculated Fe^{3+}/Fe_{Total} of 0.3–0.4 (figure 11b), even lower than in the Bishop Tuff (0.5–0.6), which crystallized near the QFM oxygen buffer (Hildreth, 1979). Thus, given the control of Fe^{3+} vs Al^{3+} by fO_2, it is possible that the low REE contents are also related to relatively low fO_2. Moreover, Fe^{3+}/Fe_{Total} in allanite from DRF-H and DRF-I indicates more reducing conditions than to DRF-A and DRF-C. Based on Fe/(Fe+Mg) ratios (figure 5), biotite in these same samples show similar relationships and substantiates the control by oxygen fugacity.

Titanite

Titanite was only found in one sample of one ash bed, DRF-I from the upper Dry Gulch Creek Member. It occurs as isolated, euhedral grains that lack clear evidence of a detrital origin but is also distinct from other volcanic titanites. Titanite in DRF-I has an average composition of $Ca_{0.99}Ti_{0.91}Si_{0.98}O_{0.96}F_{0.04}$ with only minor substitutions for Ca, Ti, and Si. Its major element composition is similar to other volcanic titanites in the database of Kowallis and others (2019). However, Fe and Al are lower than most other volcanic titanites with average Fe+Al at 0.078 apfu compared with 0.11 apfu for titanite in other silicic tuffs (figure 13). It also has distinctively low Y and Mn and a high Nb/Y ratio, a characteristic shared by the whole-rock composition. These titanite grains have LREE + Y patterns similar to these other tuffs but with lower REE values and somewhat steeper slopes from La to Y (figure 12). The LREE/Y ratio of about 9.6 from titanite in DRF-I is higher than Cenozoic Great Basin tuffs, which typically have LREE/Y of about 3.6.

The presence of titanite contradicts the evidence from biotite and allanite that the source magma was a reduced, low-temperature, rhyolitic magma, with low LREEs. Elevated Fe/(Mg+Fe) ratios in biotite and low calculated Fe^{3+}/Fe_{Total} ratios in allanite indicate fairly reducing conditions but this is unusual for titanite-bearing magmas that typically indicate oxidizing conditions. For example, Christiansen and others (2015) noted that the tuffs from the Morrison Formation containing titanite were more oxidized than tuffs without titanite, as indicated by high Mg/Fe ratios in biotite. The opposite relationship is seen in the Duchesne River Formation biotites associated with titanite, which have $\log(X_{Mg}/X_{Fe})$ ratios around -0.2 as opposed to 0.1–0.43 for Duchesne River tuffs that lack titanite (figure 9). These contradictions of oxidizing vs. reducing conditions, along with the atypical compositions discussed above and shown on figure 13, and the fact that titanite was only found in DRF-I but not DRF-H (same tuff bed) probably indicate that the titanite grains are detrital rather than a magmatic component of the tuff.

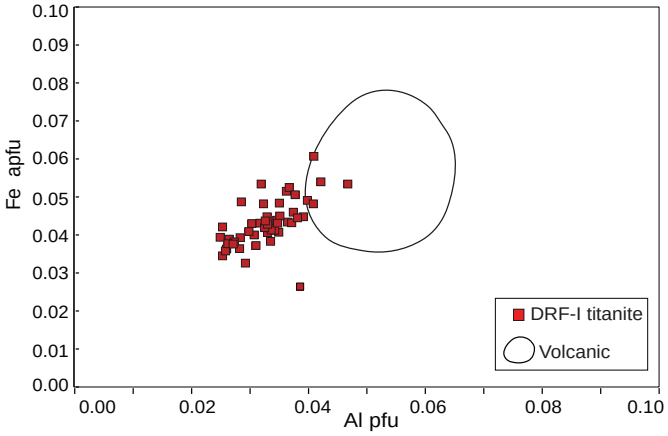

Figure 13. Compositions of titanite from the Duchesne River Formation. DRF-I titanites are depleted in both Al and Fe compared to volcanic titanite from the Cenozoic tuffs compiled by Kowallis and others (personal communication) and are probably detrital.

Apatite

Apatite was only found in one tuff, DRF-D, and proved to be significantly weathered despite a euhedral and prismatic appearance. The average analytical total was 93.56% and P_2O_5 and CaO were several weight percent lower on average than is typical for apatite. F was very high, making up as much as 4.35 wt.% of the apatite grains, a strong indication of alteration (Deer and others, 1997). DRF-D has a strong detrital component and these apatite grains may be further evidence of detrital mixing.

WHOLE-ROCK COMPOSITION

Whole-rock data was gathered using XRF techniques as well as microprobe analysis of glass shards from sample DRF-A. Whole-rock compositions provide insights about the altered and original composition of the tuffs. Analytical totals from the whole-rock XRF analyses are good (>99.74 wt.%), but loss on ignition (LOI) ranges from 4.8 wt.% all the way up to 18 wt.% for DRF-C and DRF-J. However, most samples had LOI measurements less than 9% as shown in table 4. Samples with high LOIs also show abnormally high CaO concentrations and the samples may have been contaminated with detrital carbonate despite soaking the samples in an acid bath during preparation.

Some glass shards managed to survive diagenesis

Table 4. X-ray fluorescence analyses of altered tuffs from the Duchesne River Formation.

Sample	DRF-A	DRF-B	DRF-C	DRF-D	DRF-E	DRF-F	DRF-G	DRF-H	DRF-I	DRF-J	DRF-K
Member	Tdl	Tdl	Tdl	Tdl	Tdl	Tdl	Tdl	Tdd	Tdd	Tdd	Tdd
Major Oxides											
SiO_2	71.81	59.62	52.7	68.84	73.86	70.11	65.58	67.37	66.66	54.16	73.62
TiO_2	0.44	0.38	0.4	0.51	0.53	0.31	0.38	0.24	0.18	0.21	0.3
Al_2O_3	14.91	17.57	16.74	17.6	13.29	15.41	16.45	21.29	21.34	14.64	7.55
Fe_2O_3	3.08	3.14	3.64	2.99	3.46	2.67	3.24	2.33	2.51	1.99	1.72
MnO	0.04	0.08	0.27	0.01	0.02	0.02	0.07	0.01	0.01	0.27	0.06
MgO	1.6	5.69	5.78	5.2	3.08	4.6	4.91	5.35	5.83	4.8	2.32
CaO	2.97	10.74	19.79	2.54	2.4	3.41	6.84	1.76	1.74	21.42	12.23
Na2O	2.06	1.71	0.09	0.91	0.66	1.47	0.91	0.61	1.08	1.29	0.17
K_2O	2.98	0.93	0.45	1.25	2.39	1.88	1.51	0.99	0.61	1.14	1.81
P_2O_5	0.11	0.13	0.13	0.16	0.32	0.12	0.11	0.07	0.04	0.07	0.24
LOI	4.83	12.06	18.97	7.37	5.44	7.28	9.94	8.69	8.55	18.21	11.09
Analysis Total	99.99	99.74	100.3	99.93	99.97	99.92	100.01	99.91	99.94	99.94	100.16
Trace Elements											
Sc	8	7	6	6	9	5	8	4	3	1	9
V	37	53	48	45	55	39	46	14	12	21	38
Cr	22	10	22	22	40	18	20	9	4	11	27
Ni	9	10	17	11	15	12	17	17	12	9	12
Cu	10	10	13	13	16	7	9	10	6	8	17
Zn	60	60	74	58	55	64	82	60	59	47	44
Ga	18	15	20	18	16	19	21	19	19	14	9
Rb	126	39	39	42	81	45	44	41	23	34	52
Sr	352	217	225	276	205	222	255	239	268	252	127
Y	18	17	21	21	41	18	16	6	5	30	16
Zr	174	135	140	150	153	135	122	103	88	104	182
Nb	13	12	13	14	12	9	10	18	18	11	7
Ba	750	421	179	184	280	432	363	68	48	193	189
La	28	22	22	33	44	23	27	12	11	26	25
Ce	56	52	43	64	83	44	52	23	27	47	40
Nd	25	16	7	30	43	24	25	15	16	4	9
Sm	6	4	3	7	8	6	5	5	5	2	2
Pb	22	27	21	23	19	21	24	33	35	24	12
Th	13	16	13	14	11	9	11	17	16	12	9
U	4	7	2	4	3	3	5	2	2	5	3

Note: Major oxides are in wt% and trace elements are reported in ppm. Tdl-Lapoint Member, Tdd-Dry Gulch Creek Member, LOI-loss on ignition. Normalized to 100% on a volatile free basis.

in sample DRF-A from the middle part of the Lapoint Member. DRF-A is the least altered of the all the Duchesne River Formation tuffs based on SiO_2 levels in the glass and immobile elements such as Nb, Zr, and Ti. The electron microprobe analyses indicate these shards are high-silica rhyolite with SiO_2 >75% with low concentrations of TiO_2, Fe_2O_3, and MgO when normalized to 100% on a volatile free basis (see the supplemental data file).

Immobile Elements

Given the altered condition of the Duchesne River Formation tuffs and likely contamination from detrital material, whole-rock compositions do not represent the original composition of the volcanic ash. However, by comparing immobile elements such as Nb, Zr, Ti, and REE, some information about the initial composition can be determined. Even though immobile element concentrations will typically be changed by alteration, they are similarly enriched or depleted so that ratios of

these elements can still be used to make general inferences about the original composition and volcanic setting (Kowallis and others, 2001; Christiansen and others, 2015). TiO_2/Al_2O_3 ratios in altered ash beds from terrestrial settings can also be used to determine the extent of physical reworking and chemical alteration and TiO_2/Al_2O_3 values <0.055 are indicative of primary ash composition (Hong and others, 2019). Despite extensive argillic alteration seen in most of the Duchesne River Formation tuffs (discussed below) all the tuffs appear to have maintained a TiO_2/Al_2O_3 ratio <0.055.

On the discrimination diagrams of Winchester and Floyd (1977), the Duchesne River Formation tuffs plot in the dacite and rhyolite fields based on Nb/Y vs. Zr/Ti (figure 14a). Samples DRF-H and DRF-I have anonymously low Y resulting in high Nb/Y ratios so they plot in the trachyte field, but their Zr/Ti ratios are rhyolitic. The distinctive low Y content could be the result of pre-eruptive fractionation of titanite and allanite which are both present in the tuff and have high partition coefficients for Y. (As noted earlier, the titanite in this sample also has an anomalously high Nb/Y ratio.) When Zr/Ti is plotted against Ce ppm, all of the Duchesne River samples plot in the rhyolite field (figure 14b) which agrees with the fresh glass analysis and the mineral assemblages and compositions (e.g., sodic sanidine, quartz, low Ti biotite).

Tectonic setting can also be inferred from immobile elements and careful use of some mobile trace elements. Figure 15 shows discrimination plots by Pearce (1984) that compare Nb, Y, and Rb concentrations. Both diagrams show that the Duchesne River Formation tuffs have compositions characteristic of a volcanic arc setting, assuming the elements plotted have not been significantly changed by alteration. A volcanic arc setting also agrees with trace element patterns of the Duchesne River Formation tuffs (figure 16) which are typical of subduction-related calc-alkaline magmas including large negative Nb anomalies, strong positive Pb anomalies, and a generally decreasing trend from left to right. Average abundances of trace elements from volcanic arc tuffs that also experienced argillic alteration (described below) from the Jurassic Morrison Formation (Christiansen and others, 2015) are plotted as a comparison to the Duchesne River tuffs.

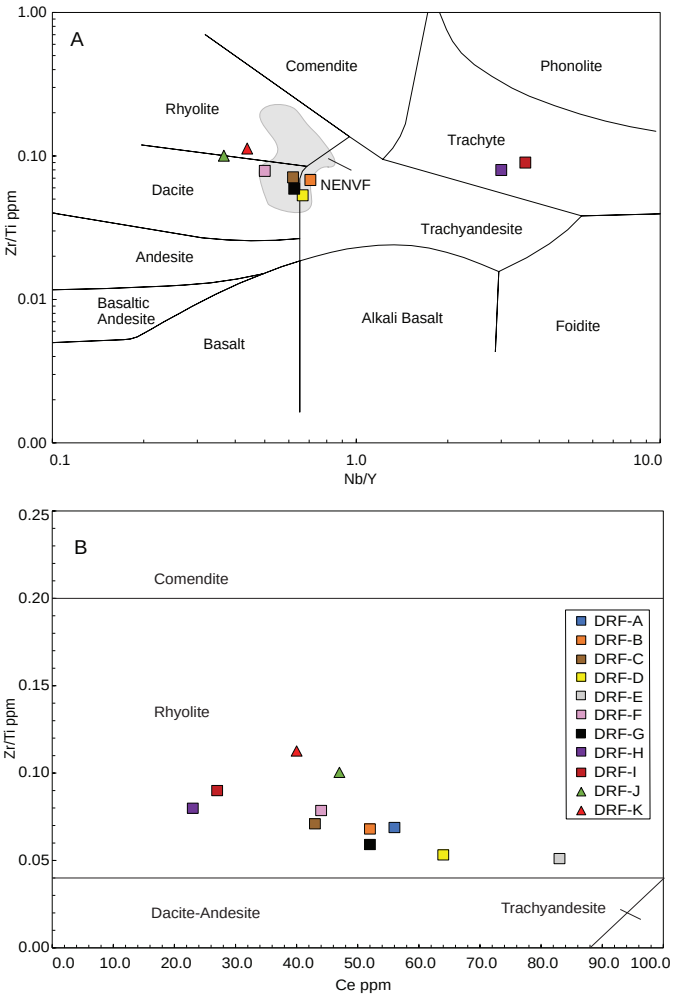

Figure 14. (A) Immobile element diagram modified from Winchester and Floyd (1977). Duchesne River Formation tuffs all plot in the rhyolite field. Ce has not been reported for the northeast Nevada volcanic field. (B) Most of the tuffs plot in the dacite and rhyolite field. DRF-H and DRF-I have anomalously low Nb/Y ratios. Unaltered ignimbrite compositions from the northeast Nevada volcanic field (NENVF) are shown for comparison (Brooks, 1995a).

Argillic Alteration

The extensive secondary alteration exhibited by the Duchesne River Formation tuffs can provide insight into the depositional environment (Christiansen and others, 2015). All the tuffs exhibit signs of argillic alteration to swelling clays as is typical of the alteration of volcanic glass. SiO_2 values range from 68% in DRF-A all the way to 42% in DRF-C, all low for rhyolite magmas

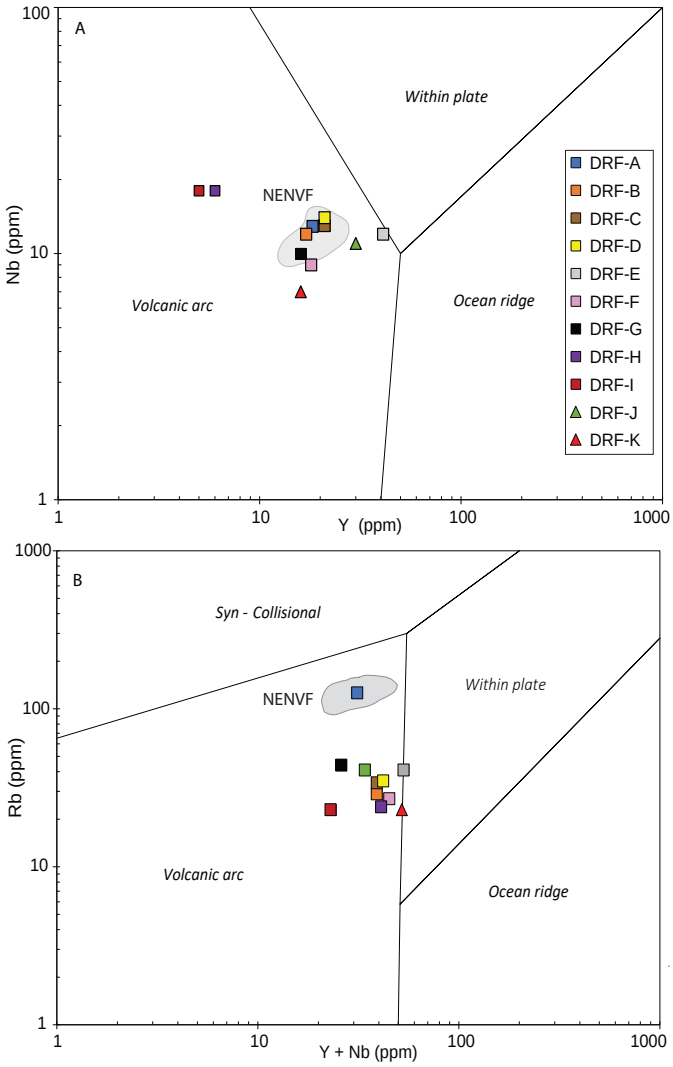

Figure 15. Trace element discrimination diagrams from Pearce and others (1984). (A) Nb vs. Y. Duchesne River Formation and northeast Nevada volcanic field (NENVF) tuffs plot in the volcanic arc field and are almost identical except for two anomalously low Y samples. (B) Rb vs. Y+Nb Duchesne River Formation tuffs and NENVF tuffs plot in the volcanic arc field. Rb is probably low in most samples because of secondary alteration.

which typically have SiO_2 values in the low to mid 70s. Al_2O_3 tends to increase as SiO_2 decreases in the altered Morrison Formation tuffs and a similar trend occurs in the Duchesne River Formation samples (figure 17). Argillic alteration also causes an increase in MgO as SiO_2 is removed, but the opposite relationship is seen in feldspathically altered tuffs, which have relatively low MgO and high SiO_2.

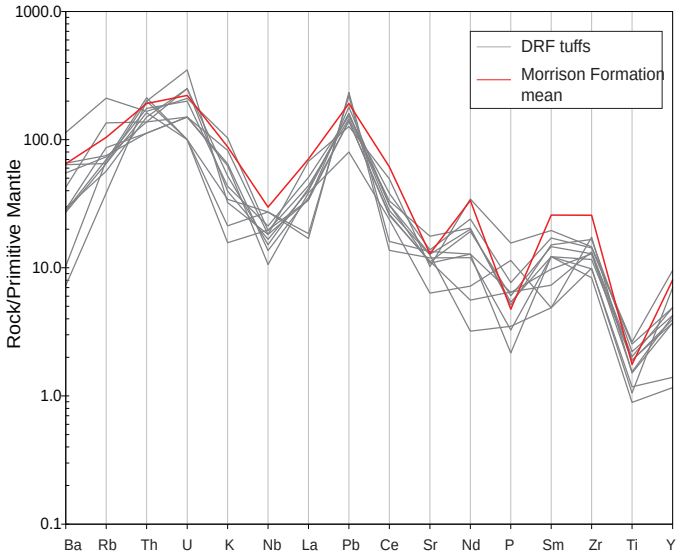

Figure 16. Trace element patterns normalized to primitive mantle (McDonough and Sun, 1994) for bentonitic tuffs from the Duchesne River Formation and the average argillically altered tuff from the Morrison Formation. The Duchesne River tuffs and Morrison tuff average are similar and have general patterns typical of a continental subduction zone setting. The irregularity of some of the patterns is probably the result of secondary alteration, e.g., Ba, Rb, La, Nd, and P are quite variable.

Another important effect of the diagenesis of the tuffs was the deposition of carbonate minerals. The high CaO content (table 4) in the tuffs is as high as 20 wt.%; a normal rhyolite would have about 1 wt.%. Carbonate precipitation significantly diluted the less mobile elements like Al_2O_3 and SiO_2.

The presence of argillic alteration of the tuffs, an indication of a freshwater setting (Christiansen and others, 2015), agrees with sedimentologic evidence on the depositional environment of the Duchesne River Formation in a freshwater fluvial/wetland setting (Andersen and Picard, 1972, 1974; Sato and Chan, 2015; Webb, 2017). Carbonates also formed and filled the pore spaces during diagenesis.

DISCUSSION

Eruptive Source of the Duchesne River Formation Tuffs

Age, inferred original composition, eruption type,

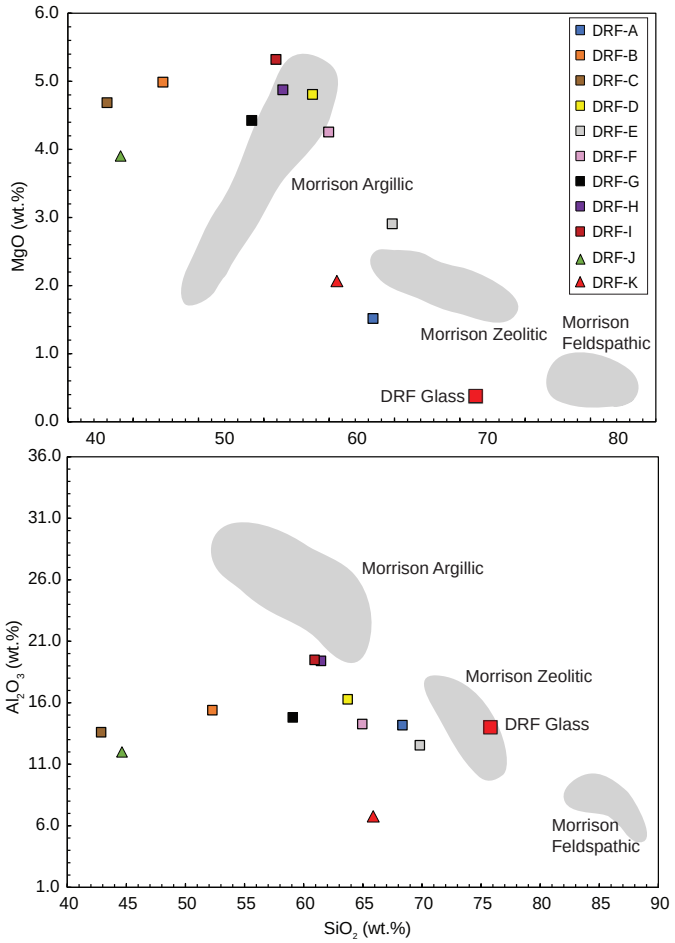

Figure 17. Two element diagrams of the Duchesne River Formation tuffs and fields for Morrison Formation tuffs showing the different effects of alteration type on major elements. The composition of the glass from DRF-A is plotted as representative of the original unaltered composition of the tuffs. The Duchesne River Formation and Morrison Formation argillic samples show similar patterns of SiO_2 depletion and MgO and Al_2O_3 enrichment. Morrison Formation feldspathic samples show the opposite relationship of argillic and zeolitic samples which show little change in Al_2O_3 but significant additions of MgO—neither of which apply to the altered tuffs of the Duchesne River Formation.

and geographic location are the main criteria we have used to try to identify eruptive sources for the ash beds within the Duchesne River Formation. Any potential source would need to have erupted within a narrow age range around 39.4 Ma, have a high-silica, calc-alkaline composition, be capable of producing large Plinian eruptions, and lie to the west of the Uinta Basin where prevailing winds could transport the ash east to eventually be deposited.

Several large volcanic fields in western North America (figure 1) might have been eruptive sources for the Duchesne River Formation tuff beds. These include the northeast Nevada (Brooks and others, 1995a, 1995b; 1995c; Rahl and others, 2002), Tuscarora (Henry and others, 1998; Smith and others, 2017), Absaroka (Chandler, 2006), Challis (Chandler, 2006), central Nevada (Best and others, 2009; 2013b), Indian Peak (Best and others, 2013c), and Robinson Mountain (Lund-Snee and others, 2016; Smith and others, 2017). These volcanic fields either pre-date or post-date the Duchesne River Formation tuffs except for the northeast Nevada and Tuscarora fields. Ages of volcanic, volcaniclastic, and plutonic rocks of the Tuscarora volcanic field range from about 41 to 39 Ma (Coats and McKee, 1972; Berger and others, 1991; Henry and others, 1999; Castor and others, 2003; Henry, 2008). However, the only known large ash-flow tuff from this field, the tuff of Big Cottonwood Canyon, has a well-established age of 39.92 to 40.15 ± 0.10 Ma (Henry, 2008), recalculated for a Fish Canyon age of 28.201 Ma. Comparing these ages to our new ages on the Duchesne River Formation tuffs ($^{40}Ar/^{39}Ar$ ages of 39.47 ± 0.16 Ma and 39.36 ± 0.15 Ma) shows that the tuff of Big Cottonwood Canyon is older.

The Keetley Volcanics (Crittenden and others, 1973; Bromfield and others, 1977; Constenius and others, 2011), Tintic Mountain Volcanic Group (Moore, 1973; Keith and others, 1989), Marysvale volcanic field (Rowley and others, 2002), and volcanic rocks of the Thomas caldera in north and central Utah are hundreds of kilometers closer to the Uinta Basin than those in Nevada but are several million years too young to be considered correlative as illustrated on figure 18 and summarized in table 5. Figure 18 also lists possible intrusive complexes that could be considered as the source for the Duchesne River Formation tuffs. However, the ages we have obtained on the tuffs do not match any of these regional intrusive complexes except the Bingham intrusive complex in northern Utah which was active from 39.18 to 37.2 Ma (Warnaars and others, 1978; Deino and Keith, 1997). The composition of the Bingham stock is more primitive and mafic and includes monzonite, quartz monzonite, and quartz latite with hornblende and py-

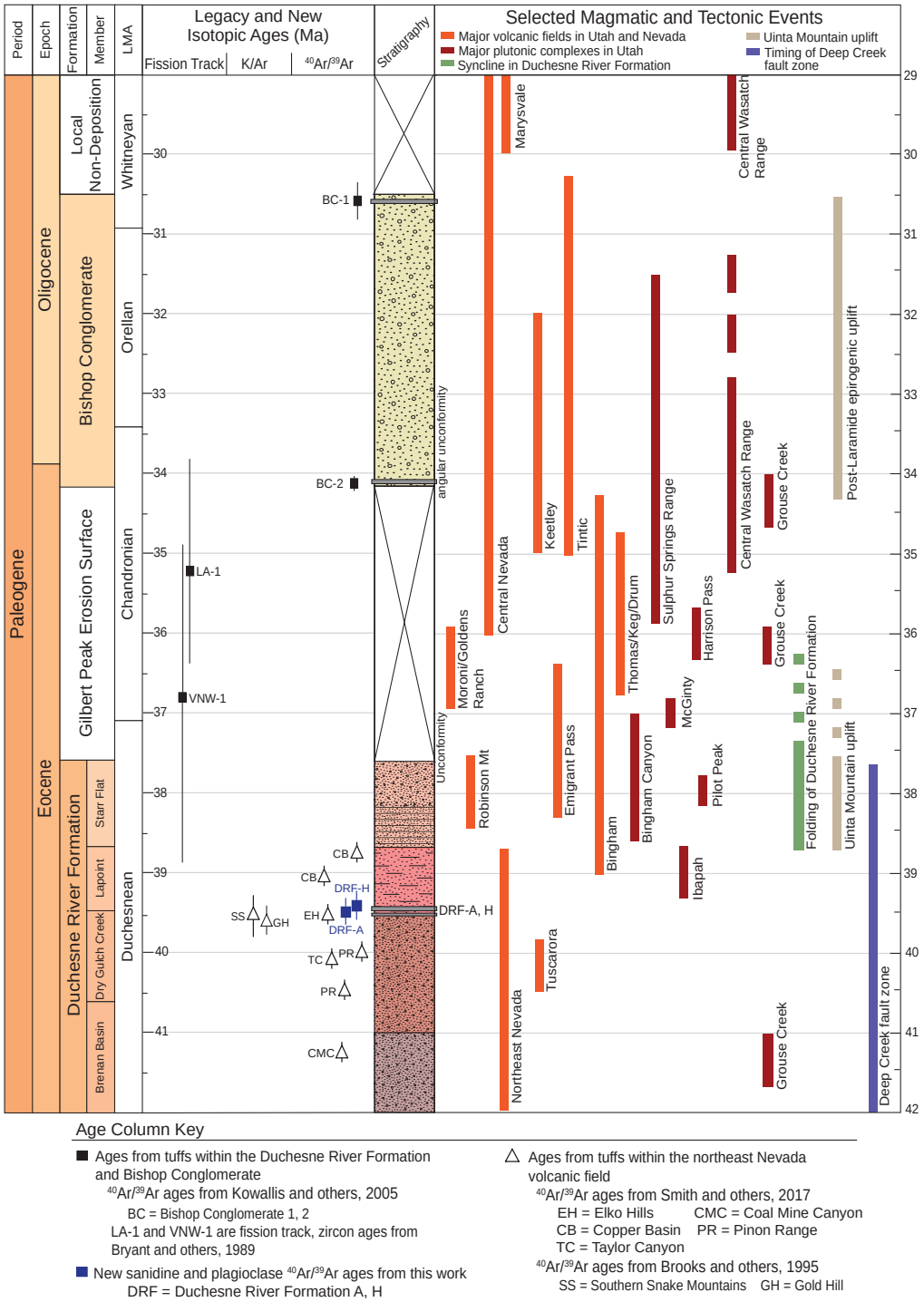

Figure 18. Timeline illustrating the sequence of major regional magmatic and tectonic events in Utah and Nevada, as well as local events in the Uinta Basin area. The ages of the volcanic and plutonic events (orange and red lines) indicate that the northeast Nevada volcanic field is the most likely volcanic source of the Duchesne River Formation tuffs. References for the ages of volcanic fields and plutonic complexes are listed in table 5. U-Pb ages and K-Ar ages are included to show the large errors in the previously used ages. Other $^{40}Ar/^{39}Ar$ ages from various tuffs from the northeast Nevada volcanic field are plotted to demonstrate the volcanic activity of the northeastern Nevada region at this time. Folding of the Duchesne River Formation took place over a short span of time and was likely coeval with the deposition of the Starr Flat Member.

Table 5. List of magmatic events, ages, and references used on figure 18.

Plutonic Complex	Age (Ma)	Reference
Central Wasatch Range	29.45, 32.2–35.38	John and others, 1997; Biek and others, 2005; Smyk and others, 2018
Sulphur Springs Range	31.5–36.9	Ryskamp and others, 2008
Grouse Creek	34.3, 36.3, 41.3	Egger, 2003; Strickland and others, 2011
Harrison Pass	36	Barnes and others, 2001
Bingham Canyon	37.0–38.6	Warnaars, 1978; Deino and Keith, 1997; Vogel and others, 2001
McGinty	37	Hintze and Kowallis, 2009
Pilot Peak	37.7–38.2	Wooden and others, 1999; Woodburne, 2004
Ibapah	39	Hintze and Kowallis, 2009
Volcanic Field	Age (Ma)	Reference
Central Nevada	18–36	Best and others, 2013; Christiansen and others, 2015
Tintic	30.3–35	Keith and others, 1989
Marysvale	31–35	Rowley and others, 2002
Keetley	32–35	Constenius and others, 2011; Smyk and others, 2018
Bingham	34.2–39	Moore, 1973; Biek and others, 2005
Thomas/Keg/Drum	34.92–36.77	Shubat and Snee, 1992
Goldens Ranch/Moroni	35.9–39.9	Hintze and Kowallis, 2009
Emigrant Pass	36.4–38.2	Egger, 2003; Johnson, 2015
Robinson Mountain	37.5–38.5	Lund-Snee and others, 2015
NE Nevada	39–42.6	Brooks, 1995b; Smith and others, 2017
Tuscarora	39.8–40.5	Henry and others, 1995; Henry, 2008

Note: The Central Wasatch Range plutonic complex includes the Clayton Peak, Alta, Little Cottonwood, Flagstaff, Mayflower, Ontario, Glencoe, Valeo, Pine Creek, and Park Premier stocks.

roxene (Moore, 1973; Waite and others, 1997), minerals that are entirely absent in the Duchesne River Formation tuffs. This suggests that the Bingham stock is an unlikely intrusive counterpart to the Duchesne River Formation tuffs. The volcanic rocks associated with the Bingham intrusion also have a more mafic composition except for some rhyolitic lava flows which erupted near the end of volcanic activity around 33 Ma.

Another potential source is the volcanism in northeast Nevada. Coats (1964) mapped several tuffs in the Jarbidge quadrangle along the Nevada-Idaho border. The oldest of these, the Dead Horse Formation (Smith and others, 2017), is a composite unit composed of several ash-flow tuffs including rhyolitic tuffs with a phenocryst assemblage (quartz, biotite, sanidine, plagioclase, apatite, zircon, and allanite) similar to the Duchesne River Formation tuffs. The recalibrated ages of the tuffs in the Dead Horse Formation range from 47.61 ± 0.4 to 34.97 ± 0.25 Ma (Smith and others, 2017), overlapping the range of the Duchesne River Formation. Brooks and others (1995a, 1995b, 1995c) determined the compositions and ages of a number of ash-flow tuffs in the northeast Nevada volcanic field. $^{40}Ar/^{39}Ar$ ages from sanidine show that, of the multiple ash-flow tuffs in this volcanic field, several have ages with errors that overlap the 39.47 and 39.36 Ma ages reported in this paper for Duchesne River Formation tuffs. Based on age and compositional constraints, the most likely place to look for a source of the Duchesne River Formation tuffs is in the northeast Nevada volcanic field.

The northeast Nevada field tuffs are silicic to intermediate composition, calc-alkaline tuffs, and have similar mineral assemblages including quartz, biotite, and feldspar. Whole-rock comparisons between the Duchesne River Formation and northeastern Nevada tuffs also show similar abundances of major and trace elements. For example, Nb/Y and Zr/Ti ratios of altered Duchesne River Formation tuffs are similar to those from the northeast Nevada volcanic field (Brooks and others, 1995a, 1995c) (figure 14a). A plot of Nb vs. Y

(figure 15a) also shows that the Duchesne River Formation tuffs have compositions similar to the northeast Nevada volcanic field. However, Rb (ppm) levels in Duchesne River Formation tuffs are lower than in the northeast Nevada volcanic field (figure 15b), probably due to leaching of Rb during alteration. The least altered tuff which retains glass shards (DRF-A) seems to have retained its initial Rb concentrations, however, and plots near the volcanic rocks from the northeast Nevada volcanic field. Similar compositional data on the tuff beds in the nearby Dead Horse Formation of northern Nevada are lacking.

Aside from correlating with other igneous units to determine the eruptive source of the tuffs, compositional data can be used to make interpretations about the tectonic setting and eruptive conditions. The mineral assemblage, mineral compositions, eruption temperatures, and whole-rock compositions of the Duchesne River Formation tuffs indicate a rhyolite-dacite composition and the immobile trace element plots provide evidence for a typical continental subduction-zone tectonic setting. There is no evidence of intraplate, A-type or extension-related magmatism in these tuffs. The rhyolitic magmas from which these fall-out tuffs originated were likely generated as the subducting Farallon slab foundered and rolled back at the close of the Laramide orogeny (Best and others, 2016).

Timing of Uinta Mountain Uplift

The high-precision ages of the tuffs in the Duchesne River Formation also place important constraints on the tectonic history of the region. We propose that after a time of relative tectonic quiescence when the Brennan Basin, Dry Gulch Creek, and Lapoint Members were deposited, a renewed Laramide uplift began in the Uinta Mountains about 39 Ma, as illustrated on figure 18. The cessation of the uplift event is loosely constrained by a U-Pb zircon age of 37 ± 1.5 Ma from a tuff in the Starr Flat Member (Bryant and others, 1989). This uplift event created a syncline in the Duchesne River Formation, which dips to the south 1 to 9°, proximal to the Uinta Mountains to the north, and then dips to the north 1 to 3° farther south in the Uinta Basin (figure 1b). Uplift was followed by the development of an unconformity called the Gilbert Peak erosion surface that formed over a period of approximately 4 million years during which uplift and deposition apparently slowed and erosion dominated (Webb, 2017). The Bishop Conglomerate was deposited around 34 to 30 Ma (Kowallis and others, 2005) atop the Gilbert Peak erosion surface with some angular discordance between it and the underlying Duchesne River Formation members (figure 2). Hansen (1986), Dickinson and others (1988), Aslan and others (2017), and Sprinkel (2018a) all interpreted the Gilbert Peak erosion surface as the end of the Laramide in the Uinta Basin. Although evidence of post-Laramide but pre-extensional tectonic activity is seen throughout the Uinta Mountains, it is likely caused by epeirogenic regional uplift of the Uinta Mountains and nearby Rocky Mountains (Sprinkel, 2014, 2018a; Aslan and others, 2017). Hansen (1986) also considered changing climate conditions from warm and humid to cool and dry to explain the existence and composition of the Bishop Conglomerate.

Duchesnean North American Land Mammal Age

The Duchesne River Formation, near the town of Lapoint, Utah, is the type section of the Duchesnean NALMA (Emry, 1981), which extends from 42 to 38 Ma (Alroy, 2000). Some disagreement has arisen over the numerical age of the fauna that define the age, and whether the fauna is entirely late Eocene or part Eocene and part Oligocene (Emry, 1981; Prothero, 1995; Rasmussen and others, 1999). The majority of fossils collected from the Duchesne River Formation come from the Brennan Basin and Lapoint Members (Rasmussen and others, 1999; Burger and Tacket, 2014). The Carnegie titanothere quarry (Un0012) is stratigraphically located in the lower Lapoint Member and the Halfway Hollow quarry (Un0117) is stratigraphically located in the uppermost Dry Gulch Creek Member (figure 2). However, the Halfway Hollow quarry was originally reported to be in the lower Lapoint Member (Emry, 1981). Workers have relied on old isotopic ages taken from tuffs within these members to constrain the age of the fauna (Lucas and Emry, 2004). These old and imprecise radiometric dates have been the main reason for

the confusion about the age of the fauna. An $^{40}Ar/^{39}Ar$ age of 41.10 ± 0.32 Ma and a U-Pb zircon age of 40.66 ± 1.88 Ma were reported from the Brennan Basin Member (Sprinkel, 2018a). More importantly, two $^{40}Ar/^{39}Ar$ ages of 39.47 ± 0.16 and 39.36 ± 0.15 Ma from the Lapoint (sample DRF-A) and Dry Gulch Creek (sample DRF-H) Members are reported in this study. The 34.03 ± 0.04 Ma age of the tuff in the lower part of the overlying non-Duchesnean Bishop Conglomerate (Kowallis and others, 2005) is conclusive evidence that the faunas found within the Duchesne River Formation are entirely late Eocene which, according to the official time scale of the International Commission on Stratigraphy, ended about 33.9 Ma.

CONCLUSIONS

The Duchesne River Formation is an important fluvial-lacustrine deposit that records the uplift and development of the Uinta Mountains, a Laramide-age uplift in eastern Utah. Two key fallout tuff beds in the Duchesne River Formation give $^{40}Ar/^{39}Ar$ ages on feldspars of 39.47 ± 0.16 Ma and 39.36 ± 0.15 Ma. The tuffaceous layers in the Lapoint Member are concentrated in the lower and middle part of that member, and the tuffs from the Dry Gulch Creek Member lie in the upper and middle parts. These new ages from the Duchesne River Formation constrain a period of Laramide uplift of the Uinta Mountains from about 39 to 37 Ma.

The compositions of the phenocrysts in the thin (0.25–5.5 m) tuffs are typical of rhyolitic subduction-related magmas. The mineral assemblage of quartz, biotite, feldspar, with accessory zircon, and allanite is typical for calc-alkaline magmas. However, calculated temperatures from biotite and feldspar along with relatively low Ti and REE concentrations in allanite suggest that the magmas were cooler and less oxidized than typical arc rhyolites. Biotite compositions suggest that the parent magmas evolved compositionally over time (figure 7). The tuffs fell into fresh-water environments and the glass altered to clay, but most of the phenoclasts survived. Whole-rock compositions of the tuffs are typical of argillically altered rhyolite, indicated by an enrichment of Al and Mg, depletion of Si and K, stable levels of Nb, Y, Ti, Zr, and REE, and formation of smectitic and illitic clays as a result of the diagenesis of the volcanic glass. The immobile trace element patterns are typical of rhyolites produced in a subduction zone.

Based on age, composition, eruption style, and geographic location, the northeast Nevada volcanic field is the most likely source of the Duchesne River Formation tuffs. Other potential sources are too old or too young or have different eruptive compositions. These tuffs are distal equivalents of slab rollback-related volcanism as it flared up in northern Nevada in the late Eocene.

The faunas of the Duchesne River Formation, which define the Duchesnean NALMA, are about 39.4 Ma. This is younger than the previously published age of 41.0 Ma (Rasmussen and others, 1999). Based upon our new ages and ages reported earlier from the overlying Bishop Conglomerate, the Duchesnean NALMA is middle Eocene.

ACKOWLEDGMENTS

Funding for the project was provided by the Department of Geological Sciences and College of Physical and Mathematical Sciences at Brigham Young University. Additional support was given by the Utah Geological Survey (UGS). Assistance with sample preparation and XRF analyses was provided by David Tomlinson (Rio Tinto Kennecott). Martha Hayden (UGS) provided us with quarry locations so we could compare the stratigraphic position of the quarry to our sample locations. We thank the following for their reviews and technical editing: Grant Willis, Stephanie Carney, and Michael Hylland (UGS) and Paul Murphey (San Diego Natural History Museum).

REFERENCES

Ague, J.J., and Brimhall, G.H., 1988, Regional variations in bulk chemistry, mineralogy, and the compositions of mafic and accessory minerals in the batholiths of California: Geological Society of America Bulletin, v. 100, p. 891–911, doi:10.1130/00167606.

Alroy, J., 2000, New methods for quantifying macroevolutionary patterns and processes: Paleobiology, v. 26, no. 4, p. 707–733.

Andersen, D.W., and Picard, M.D., 1972, Stratigraphy of the Duchesne River Formation (Eocene-Oligocene?), northern Uinta Basin, northeastern Utah: Utah Geological and Mineral Survey Bulletin 97, 29 p.

Andersen, D.W., and Picard, M.D., 1974, Evolution of synorogenic clastic deposits in the intermontane Uinta Basin of Utah, *in* Dickinson, W.R., editor, Tectonics and sedimentation: Society for Sedimentary Geology (SEPM) Special Publication 22, p. 167–189.

Aslan, A., Boraas-Connors, M., Sprinkel, D.A., Karlstrom, K.E., Heizler, M., Lynds, R., and Becker, T.P., 2017, Cenozoic collapse of the eastern Uinta Mountains and drainage evolution of the Uinta Mountains region: Geosphere, v. 14, no. 1, p. 115–140.

Barnes, C.G., Burton, B.R., Burling, T.C., Wright, J. E., and Karlsson, H.R., 2001, Petrology and geochemistry of the late Eocene Harrison Pass pluton, Ruby Mountain core complex, northeastern Nevada: Journal of Petrology, v. 42, p. 301–929.

Best, M.G., Barr, D.L., Christiansen, E.H., Grommé, C.S., Deino, A.L., and Tingey, D.G., 2009, The Great Basin altiplano during the middle Cenozoic ignimbrite flareup—insights from volcanic rocks: International Geology Review, v. 51, p. 1–45.

Best, M.G., Christiansen, E.H., and Grommé, S., 2013a, Introduction—the 36–18 Ma southern Great Basin, USA, ignimbrite province and flareup—swarms of subduction-related supervolcanoes: Geosphere, v. 9, p. 260–274, doi:10.1130/GES00870.1.

Best, M.G., Christiansen, E.H., and Grommé, S., 2013b, The 36–18 Central Nevada ignimbrite field and calderas, Great Basin, USA—multicyclic super-eruptions: Geosphere, v. 9, p. 1562–1636, doi:10.1130/GES00945.1.

Best, M.G., Christiansen, E.H., and Grommé, S., 2013c, The 36–18 Indian Peak-Caliente ignimbrite field and calderas, southeastern Great basin, USA—multicyclic super-eruptions: Geosphere, v. 9, p. 864–950, doi:10.1130/GES00902.1.

Best, M.G., Christiansen, E.H., de Silva, S., and Lipman, P.W., 2016, Slab-rollback ignimbrite flare-ups in the southern Great Basin and other Cenozoic American arcs—a distinct style of arc volcanism: Geosphere, v. 12, p. 1097–1135, doi:10.1130GES01285.1.

Biek, R.F., Solomon, B.J., Keith, J.D., and Smith, T.W., 2005, Geologic map of the Tickville Spring quadrangle, Salt Lake and Utah Counties, Utah: Utah Geological Survey Map 214, 2 plates, scale 1:24,000.

Bisdom, E.B.A., Stoops, G., Delvigne, J., Curmi P., and Altemuller, H.J., 1982, Micromorphology of weathering biotite and its secondary products: Pedologie, v. 32, p. 225–251.

Blaylock, G.W., 1998, Probable correlation of the Oligocene Whitney Ash beds of western Nebraska to ash-flow tuffs in Nevada and Utah: Provo, Utah, Brigham Young University, M.S. thesis, 45 p.

Bromfield, C.S., Erickson, A.J., Jr., Haddadin, M.A., and Mehnery, H.H., 1977, Potassium-argon ages of intrusion, extrusion, and associated ore deposits, Park City mining district, Utah: Economic Geology, v. 72, p. 837–848.

Brooks, W.E., Thorman, C.H., and Snee, L.W., 1995a, The $^{40}Ar/^{39}Ar$ ages and tectonic setting of the middle Eocene northeast Nevada volcanic field: Journal of Geophysical Research, v. 100, p. 10,403–10,416.

Brooks, W.E., Thorman, C.H., and Snee, L.W., 1995b, Correction to the $^{40}Ar/^{39}Ar$ ages and tectonic setting of the middle Eocene Northeast Nevada volcanic field: Journal of Geophysical Research, v. 100, p. 15,545–15,548.

Brooks, W.E., Thorman, W.E., Snee, L.W., Nutt, C.W., Potter, C.J., and Dubiel, R.F., 1995c, Summary of chemical analyses and $^{40}Ar/^{39}Ar$-spectra data for Eocene volcanic rocks from the central part of the Northeast Nevada volcanic field: U.S. Geological Survey Bulletin 1988-K, p. K1–K33.

Bryant, B., Naeser, C.W., Marvin, R.F., and Mehnert, H.H., 1989, Upper Cretaceous and Paleogene sedimentary rocks and isotopic ages of Paleogene tuffs, Uinta Basin, Utah: U.S. Geological Survey Bulletin 1787, p. J1–J22.

Burger B.J., and Tacket, L., II., 2014, The stratigraphic importance of the brontothere (cf. *Diplacodon elatus*) in the Brennan Basin Member of the Duchesne River Formation of Utah: Fossil Record, v. 17, p. 69–74.

Carroll, A.R., and Bohacs, K.M., 1999, Stratigraphic classification of ancient lakes—balancing tectonic and climatic controls: Geology, v. 27, p. 99–102.

Castor, S.B., Faulds, J.E., Fowland, S.M., and dePolo, C.M., 2000, Geologic map of the Frenchman Mountain quadrangle, Clark County, Nevada: Nevada Bureau of Mine and Geology Maps 127, 15 p., scale 1:24,000.

Castor, S.B., Boden, D.R., Henry, C.D., Cline, J.S., Hofstra, A.H., McIntosh, W.C., Tosdal, R.M., and Wooden, J.P., 2003, The Tuscarora Au-Ag district—Eocene volcanic-hosted epithermal deposits in the Carlin Gold region, Nevada: Economic Geology, v. 98, p. 339–366.

Chandler, M.R., 2006, The provenance of Eocene tuff beds in the Fossil Butte Member of the Green River Formation of Wyoming—relation to the Absaroka and Challis volcanic fields: Provo, Utah, Brigham Young University, M.S. thesis, 89 p.

Chesner, C.A., and Ettlinger, A.D., 1989, Composition of volcanic allanite from the Toba Tuffs, Sumatra, Indonesia: American Mineralogist, v. 74, p. 750–758.

Christiansen, E.H., Sheridan, M.F., and Burt, D.M., 1986, The geology and geochemistry of Cenozoic Topaz rhyolites from the western United States: Geological Society of America Special Paper 205, 82 p., doi:10.1130/SPE205–p1.

Christiansen, E.H., Kowallis, B.J., Dorais, M.J., Hart, G.L., Mills, C.N., Pickard, M., and Parks, E., 2015, The record of volcanism in the Brushy Basin Member of the Morrison Formation—implications for the Late Jurassic of western North America: Geological Society of America Special Paper 513, p. 399–439, doi:10.1130/2015.2513(11).

Clark, J., Beerbower, J.R., and Kietzke, K.K., 1967, Oligocene sedimentation, stratigraphy, paleoecology and paleoclimatology in the big Badlands of South Dakota: Fieldiana Geology Memoirs, v. 5, 158 p.

Coats, R.R., 1964, Geology of the Jarbidge quadrangle, Nevada-Idaho: U.S. Geological Survey Bulletin 1141-M, p. 24

Coats, R.R., and McKee, E.H., 1972, Ages of plutons and types of mineralization, northwestern Elko County, Nevada: U.S. Geological Survey Professional Paper 800-C, p. C165–C168.

Constenius, K.N., Clark, D.L., King, J.K., and Ehler, J.B., 2011, Interim geologic map of the Provo 30' x 60' quadrangle, Salt Lake, Utah, and Wasatch Counties, Utah: Utah Geological Survey Open-File Report 586DM, 42 p., 1 plate, scale 1:62,500.

Crittenden, M.D., Stuckless, J.S., and Kistler, R.W., 1973, Radiometric dating of intrusive rocks in the Cottonwood area, Utah: Research Journal of the U.S. Geological Survey, v. 1, no. 2, p. 173–178.

DeCelles, P.G., 1994, Late Cretaceous-Paleocene synorogenic sedimentation and kinematic history of the Sevier thrust belt, northeast Utah and southwest Wyoming: Geological Society of America Bulletin, v. 106, p. 32–56.

Deer, W.A., Howie, R.A., and Zussman, J., 1997, Rock forming minerals—volume 1A, Orthosilicates (2nd edition): Bath, United Kingdom, The Geological Society, p. 663–669.

Deino, A., and Keith, J.D., 1997, Ages of volcanic and intrusive rocks in the Bingham mining district, Utah, *in* John, D.A., and Ballantyne, G.H., editors, Geology and ore deposits of the Oquirrh and Wasatch Mountains, Utah: Society of Economic Geologists Guidebook Series, v. 29, p. 91–95, doi: https://doi.org/10.5382/GB.29.

Dickinson, W.R., 2004, Evolution of the North American Cordillera: Annual Reviews of Earth and Planetary Science, v. 32, p. 13–45.

Dickinson W.R., Klute, M.A., Hayes, M.J., Janecke, S.U., Lundin, E.R., McKittrick, M.A., and Olivares, M.D., 1988, Paleogeographic and paleotectonic setting of Laramide sedimentary basins in the central Rocky Mountain region: Geological Society of America Bulletin, v. 100, p. 1023–1039.

Egger, A.E., Dumitri, T.A., Miller, E.L., Savage. C.F.I., and Wooden, J.L., 2003, Timing and nature of Tertiary plutonism and extension in the Grouse Creek Mountains, Utah: International Geology Review, v. 45, p. 497–532.

Elkins, L.T., and Grove, T.L., 1990, Ternary feldspar experiments and thermodynamic models: American Mineralogist, v. 75, p. 544–559.

Emry, R.J., 1981, Additions to the mammalian fauna of the type Duchesnean, with comments on the status of the Duchesnean "Age:" Journal of Paleontology, v. 55, p. 563–570.

Fan, M., and Carrapa, B., 2014, Late Cretaceous-early Eocene Laramide uplift, exhumation, and basin subsidence in Wyoming—crustal responses to flat slab subduction: Tectonics, v. 33, p. 509–529, doi:10.1002/2012TC003221.

Giere, R., and Sorenson, S.S., 2004, Allanite and other REE-rich epidote-group minerals: Reviews in Minerology and Geochemistry, v. 56, p. 431–493.

Hamilton, W., 1978, Mesozoic tectonics of the western U.S., *in* Howell, D.G., and McDougall, A.K., editors, Mesozoic paleogeography of the western United States: Los Angeles, California, Pacific Section, Society of Economic Paleontologists and Mineralogists, p. 33–70.

Hansen, W.R., 1986, Neogene tectonics and geomorphology of the eastern Uinta Mountains in Utah, Colorado, and Wyoming: U.S. Geological Survey Professional Paper 1356, 78 p.

Henry, C.D., 2008, Ash-flow tuffs and paleovalleys in northeastern Nevada—implications for Eocene paleogeography and extension in the Sevier hinterland, northern Great Basin: Geosphere, v. 4, p. 1–35, doi: 10.1130/GES00122.1.

Henry, C.D., Boden, D.R., and Castor, S.B., 1998, Geology and mineralization of the Eocene Tuscarora volcanic field, Elko County, Nevada, *in* Tosdale, R.M., editor, Contributions to the gold metallogeny of northern Nevada: U.S. Geological Survey Open-File Report 98-338-B, p. 279–290.

Henry, C.D., Boden, D.R., and Castor, S.C., 1999, Geologic map of the Tuscarora quadrangle, Nevada: Nevada Bureau of Mines and Geology Map 116, 20 p., scale 1:24,000,

Hildreth, E.W., 1979, The Bishop Tuff—evidence for the origin of compositional zonation in silicic magma chambers, *in* Chapin, C.E., and Elston, W.E., editors, Ash-flow tuffs: Geological Society of America Special Paper 180, p. 43–75.

Hildreth, E.W., and Wilson, C.J.N., 2007, Compositional zoning of the Bishop Tuff: Journal of Petrology, v. 48, p. 951–999, doi: 10.1093/petrology/cgm007.

Hong, H., Alego, T.J., Fang, Q., Zhao, L., Ji, K., Yin, K., Wang, C., and Cheng, S., 2019, Facies dependence of the mineralogy and geochemistry of altered volcanic ash beds—an example from Permian-Triassic transition strata in southwestern China: Earth Science Reviews, v. 190, p. 58–88.

Huff, W.D., 2016, K-bentonites—a review: American Mineralogist, v. 101, p. 43–70.

Humphreys, E.D., 1995, Post-Laramide removal of the Farallon slab, western United States: Geology, v. 23, p. 987–990.

Jensen, M.S., 2017, $^{40}Ar/^{39}Ar$ Ages, compositions, and likely source of the Eocene fallout tuffs in the Duchesne River Formation, northeastern Utah: Provo, Utah, Brigham Young University, M.S. thesis, 107 p.

Jicha, B.R., and Brown, F.H., 2014, An age for the Korath Range, Ethiopia and the viability of $^{40}Ar/^{39}Ar$ dating of kaersutite in Late Pleistocene volcanics: Quaternary Geochronology, v. 21, p. 53–57.

Jicha, B.R., Scholl, D.W., and Rea, D.K., 2009, Circum-Pacific flare-ups and global cooling near the Eocene-Oligocene boundary: Geology, v. 37, p. 303–306, doi: 10.1130/G25392A.1.

John, D.A., Turrin, B.D., and Miller, R.J., 1997, New K-Ar and $^{40}Ar/^{39}Ar$ ages of plutonism, hydrothermal alteration, and mineralization in the central Wasatch Mountains, Utah, *in* John, D.A., and Ballantyne, G.H., editors, Geology and ore deposits of the Oquirrh and Wasatch Mountains, Utah: Society of Economic Geologists Guidebook Series, v. 29, p. 47–57.

Johnson, C.L., 2015, Petrology and geochemistry of the Emigrant Pass volcanics, Nevada—implications for a magmatic-hydrothermal origin of the Carlin gold deposits: Corvallis, Oregon State University, M.S. thesis, 73 p.

Jones, C.H., Farmer, G.L., Sageman, B., and Zhong, S., 2011, Hydrodynamic mechanism for the Laramide orogeny: Geosphere, v. 7, p. 183–201, doi: 10.1130/GES00575.1.

Keith, J.D., Dallmeyer, R.D., and Kim, C.S., 1989, A re-evaluation of the volcanic history and mineral potential of the central East Tintic Mountains, Utah: Utah Geological and Mineral Survey Open-File Report 166, 90 p., 2 plates [Eureka and Tintic Mountain quadrangles], scale 1:24,000.

Kowallis, B.J., Christiansen, E.H., and Deino, A.L., 1991, Age of the Brushy Basin Member of the Morrison Formation, Colorado Plateau, western USA: Cretaceous Research, v. 12, p. 483–493, doi:10.1016/0195-6671(91)90003-U.

Kowallis, B.J., Christiansen, E.H., Deino, A.L., Peterson, F., Turner, C.E., Kunk, M.J., and Obradovich, J.D., 1998, The age of the Morrison Formation: Modern Geology, v. 22, p. 235–260.

Kowallis, B.J., Christiansen, E.H., Deino, A.L., Zhang, C., and Everett, B.H., 2001, The record of Middle Jurassic volcanism in the Carmel and Temple Cap Formations of southwestern Utah: Geological Society of America Bulletin, v. 113, p. 373–387.

Kowallis, B.J., Christiansen, E.H., Balls, E., Heizler, M.T., and Sprinkel, D.A., 2005, The Bishop Conglomerate ash beds, south flank of the Uinta Mountains, Utah—are they pyroclastic fall beds from the Oligocene ignimbrites of western Utah and eastern Nevada?, *in* Dehler, C.M., Pederson, J.L., Sprinkel, D.A., and Kowallis, B.J., editors, Uinta Mountain Geology: Utah Geological Association Publication 33, p. 131–145.

Kowallis, BJ., Hunt, J.E., Sprinkel, D.A., May, S.B., Bradfield, T.D., and Brown, K.D., 2018, Geologic map of the Lake Mountain quadrangle, Uintah County, Utah: Utah Geological Survey Miscellaneous Publication 18-2DM, 13 p., 2 plates, scale 1:24,000.

Kuiper, K.F., Deino, A., Hilgen, F.J., Krijfsman, W., Renne, P.R., and Wijbrans, J.R., 2008, Synchronizing rock clocks of earth history: Science, v. 320, p. 500–504, doi: 10.1126/science.1154339.

Lee, J.Y., Marti, K., Severinghaus, J.P., Kawamura, K., Yoo, H.S., Lee, J.B., and Kim, J.S., 2006, A redetermination of the isotopic abundances of atmospheric Ar: Geochemica et Cosmochimica Acta, v. 70, p. 4507–4512.

Lipman, P.W., Prostka, H.J., and Christiansen R.L., 1972, Cenozoic volcanism and plate-tectonic evolution of the western United States, I—early and middle Cenozoic: Philosophical Transactions Royal Society of London, v. 271, p. 217–248.

Lucas S.G., and Emry R.J., 2004, The Entolodont Brachyhyops (Mammilia Artiodactyla) from the upper Eocene of Flagstaff Rim, Wyoming, *in* Lucas, S.G., Zeigler, K.E., and Kondrashov, P.E., editors, Paleogene mammals: New Mexico Museum of Natural History and Science Bulletin 26, p. 97–101.

Liu, L., Gurins, M., Seton, M., Saleeby, J., Muller, R.D., and Jackson, J.M., 2010, The role of oceanic plateau subduction in the Laramide orogeny: Nature Geoscience, v. 3, p. 353–357, doi:10.1038/NGE0829.

Luhr, F.J., Carmichael, I.S.E., and Varekamp, J.C., 1984, The 1982 eruptions of El Chichon volcano, Chiapas, Mexico—mineralogy and petrology of the anhydrite-bearing pumices: Journal of Volcanology and Geothermal Research, v. 23, p. 69–108, doi:10.1016/0377-0273(84)90057-X.

Lund-Snee, J.E., Miller, E.L., Hourigan, J.K., and Konstantinou, A., 2016, Cenozoic paleogeographic evolution of the Elko Basin and surrounding region, northeast Nevada: Geosphere, v. 12, p. 464–500, doi: 10.1130/GE801193.1.

McDonough, W.F., and Sun, S.S., 1994, The composition of the earth: Chemical Geology Isotope Geoscience, v. 120, p. 223–253.

McDowell, F.W., Wilson, J.A., and Clark, J., 1973, K-Ar dates for biotite from two paleontologically significant localities—Duchesne River Formation, Utah, and Chadron Formation, South Dakota: Isochron/West, v. 7, p. 11–12.

Min, K., Mundil, R., Renne, P.R., and Ludwig, K.R., 2000, A test for systemic errors in $^{40}Ar/^{39}Ar$ geochronology through comparison with U/Pb analysis of a 1.1-Ga rhyolite: Geochemica et Cosmochimica Acta, v. 64, no. 1, p. 73–98.

Moore, W.J., 1973, Igneous rocks in the Bingham mining district, Utah: U.S. Geological Survey Professional Paper 629-B, 42 p.

Norman, M.D., and Mertzman, S.A., 1991, Petrogenesis of Challis volcanics from central and southwestern Idaho—trace element and Pb isotopic evidence: Journal of Geophysical Research, v. 96, p. 13,279–13,293, doi: 10.1029/91JB00285.

Pearce, J., 1984, Trace element discrimination diagrams for the tectonic interpretation of granitic rocks: Journal of Petrology, v. 25, p. 956–983.

Petrik, I., Broska, I., Lipka, J., and Siman, P., 1995, Granitoid allanite-(Ce)—substitution relations, redox conditions, and REE distributions on an example of I-type granitoids, western Carpathians, Slovakia: Geology Carpathica, v. 46, p. 79–94.

Prothero, D.R., 1995, Geochronology and magnetostratigraphy of Paleocene North American land mammal "ages"—an update: Society for Sedimentary Geology (SEPM) Special Publication 54, p. 305–316, ISBN 1-565576-024-7.

Prothero, D.R., and Swisher, C.C., III, 1992, Magnetostratigraphy and geochronology of the terrestrial Eocene-Oligocene transition in North America, *in* Prothero, D.R., and Berggren, W.A., editors, Eocene-Oligocene climatic and biotic evolution: New Jersey, Princeton University Press, p. 46–73.

Rahl, J.M., McGrew, A.J., and Foland, K.A., 2002, Transition from contraction to extension in the northeastern Basin and Range—new evidence from the Copper Mountains, Nevada: Journal of Geology, v. 110, p. 179–194.

Rasmussen, D.T., Hamblin, A.H., and Tabrum, A.R., 1999, The mammals of the Eocene Duchesne River Formation, *in* Gillette, D.D., editor, Vertebrate paleontology in Utah: Utah Geological Survey Miscellaneous Publication 99-1, p. 421–428.

Remy, R.R., 1992, Stratigraphy of the Eocene part of the Green River Formation in the south-central part of the Uinta Basin, Utah—a multidisciplinary approach to research studies of sedimentary rocks and their constituents and the evolution of sedimentary basin, both ancient and modern: U.S. Geological Survey Bulletin 1787–BB, 79 p.

Renne, P.R., Deino, A.L., Hilgen, F.J., Kuiper, K.F., Mark, D.F., Mitchell, W.S., III, Morgan, L.E., Mundil, R., and Smit, J., 2013, Time scales of critical events around Cretaceous-Paleogene boundary: Science, v. 339, p. 684–687, doi:10.1123/science.1230492.

Riggs, N.R., Ash, S.R., Barth, A.P., Gehrel, G.E., and Wooden, J.L., 2003, Isotopic age of the Black Forest Bed, Petrified Forest Member, Chinle Formation, Arizona—an example of dating a continental sandstone: Geological Society of America Bulletin, v. 115, p. 1315–1323.

Rowley, P.D., Cunningham, C.G., Steven, T.A., Workman, J.B., Anderson, J.J., and Theissen, K.M., 2002, Geologic map of the central Marysvale volcanic field, southwestern Utah: U.S. Geological Survey Geologic Investigations Series 1-2645-A, 1 plate, scale 1:62,500.

Ryskamp, E.B., Abbott, J.T., Christiansen, E.H., Keith, J.D., Vervoot, J.D., and Tingey, D.G., 2008, Age and petrogenesis of volcanic and intrusive rocks in the Sulphur Spring Range, central Nevada—comparisons with ore associated Eocene magma systems in the Great Basin: Geosphere, v. 4, p. 496–519, doi: 10.1130/GES0013.1.

Sato, T., and Chan, M.A., 2015, Source-to-sink fluvial systems for sandstone reservoir exploration—example from the basal Brennan Basin Member of Tertiary Duchesne River Formation, northern Uinta Basin, Utah, *in* Vanden Berg, M.D., Ressetar, R., and Birgenheier, L.P., editors, Geology of Utah's Uinta Basin and Uinta Basin: Utah Geological Association Publication 44, p. 91–107.

Schellart, W.P., Freeman, J., Stegman, D.R., Moresi, L., and May, D., 2007, Evolution and diversity of subduction zones controlled by slab width: Nature, v. 446, p. 308–311.

Shubat, M.A., and Snee, L.W., 1992, High-precision $^{40}Ar/^{39}Ar$ geochronology, volcanic stratigraphy, and mineral deposits of Keg Mountain, west-central Utah: U.S. Geological Survey Bulletin 2012, p. G1–G16.

Smith, M.E., Singer, B., and Carroll, A., 2003, $^{40}Ar/^{39}Ar$ geochronology of the Eocene Green River Formation, Wyoming: Geological Society of America Bulletin, v. 115, p. 549–565.

Smith, M.E., Singer, B.S., Carroll, A.R., and Fournelle, J.H., 2008, Precise dating of biotite in distal volcanic ash—isolating subtle alteration using $^{40}Ar/^{39}Ar$ laser incremental heating and electron microprobe techniques: American Mineralogist, v. 93, p. 784–795, doi:10.2138/am.2008.2517784.

Smith, M.E., Carroll, A.R., Jicha, B.R., Cassel, E.J., and Scott, J.J., 2014, Paleogeographic record of the Eocene Farallon slab rollback beneath western North America: Geology, v. 42, p. 1039–1042, doi: 10.1130/G36025.1.

Smith, M.E., and Carroll, A.R., editors, 2015, Stratigraphy and paleolimnology of the Green River Formation, western USA—syntheses in limnology 1: Dordrecht, Springer Science+Business Media, 355 p., doi: 10.1007/978-94-017-9906-5_1.

Smith, M.E., Cassel, E.J., Jicha, B.R., Singer, B.S., and Canada, A.S., 2017, Hinterland drainage and lake formation in response to middle Eocene Farallon slab removal, Nevada, USA: Earth and Planetary Science Letters, v. 479, p. 156–169, doi:10.1016/j.epsl.2017.09.023

Smyk, E., Hollings, P., Baker, M., Cooke, D.R., Thompson, J.A., Thompson, J.M., and Creaser, R., 2018, Geochemistry and geochronology of the intrusive rocks of the central Wasatch Mountains igneous belt, Utah, USA—implications for porphyry mineralization: Utah Geological Association Publication 47, p. 305–327.

Sprinkel, D.A., 2007, Interim geologic map of the Vernal 30' x 60' quadrangle, Uintah and Duchesne Counties, Utah, Moffat and Rio Blanco Counties, Colorado: Utah Geological Survey Open-File Report 506DM, compact disc, GIS data, 3 plates, scale 1: 100,000.

Sprinkel, D.A., 2014, The Uinta Mountains—a tale of two geographies and more: Utah Geological Survey, Survey Notes, v. 46, no. 3, p. 1–4.

Sprinkel, D.A., 2018a, Interim geologic map of the Duchesne 30' x 60' quadrangle, Duchesne and Wasatch Counties, Utah: Utah Geological Survey Open-File Report 689, 38 p., 2 plates, scale 1:62,500.

Sprinkel, D.A., 2018b, Mysteries of the Uinta Mountains: Utah Geological Survey, Survey Notes, v. 50, no. 3, p. 1–3.

Stoener, R.W., Schaeffer, O.A., and Katcoff, S., 1965, Half-lives of argon-37, argon-39, and argon-42: Science, v. 148, p. 1325–1328, doi:10.1123/science.148.3675.1325.

Strickland, A., Miller, E.L., and Wooden, J.L., 2011, The timing of tertiary metamorphism and deformation in the Albion-Raft River-Grouse Creek metamorphic core complex, Utah and Idaho: The Journal of Geology, v. 119, p. 185–206, doi: 10.1086/658294.

Tanavsuu-Milkeviciene, K., Sarg, J.F., and Bartov, Y., 2017, Depositional cycles and sequences in an organic-rich lake basin—Eocene Green River Formation, Lake Uinta, Colorado and Utah, USA: Journal of Sedimentary Research, v. 87, p. 210–229, doi: http://dx.doi.org/10.2110/jsr.2017.11.

Utah Geological Survey, and Apatite to Zircon Inc., 2014, U-Pb detrital zircon geochronology result for the Brennan Basin Member of the Duchesne River Formation, Duchesne 30' x 60' quadrangle, Duchesne and Wasatch Counties, Utah: Utah Geological Survey Open-File Report 635, 56 p.

Vogel, T.A., Cambray, F.W., and Constenius, K.N., 2001, Origin, and emplacement of igneous rocks in central Wasatch Mountains, Utah: Rocky Mountain Geology, v. 36, p. 119–162.

Waite, K.A., Keith, J.D., Christiansen, E.H., Whitney, J.A., Hattori, K., Tingey, D.G., and Hook, C.J., 1997, Petrogenesis of the volcanic and intrusive rocks associated with the Bingham porphyry Cu-Au-Mo deposit, Utah, *in* John, D.A., and Ballantyne, G.H., editors, Geology and ore deposits of the Oquirrh and Wasatch Mountains, Utah: Society of Economic Geologists Guidebook Series, v. 29, p. 69–90.

Ward, J.H., 1963, Hierarchical grouping to optimize an objective function: Journal of the American Statistical Association, v. 58, p. 236–244.

Warnaars, F.W., Smith, W.H., Bray, R.E., Lanier, G., and Shafiqullah, M., 1978, Geochronology of igneous intrusions and porphyry copper mineralization at Bingham, Utah: Economic Geology, v. 73, no. 7, p. 1242–1249.

Warner, M.M., 1966, Sedimentational analysis of the Duchesne River Formation, Uinta Basin, Utah: Geological Society of America Bulletin, v. 77, p. 945–958.

Webb, C.A., 2017, Geologic mapping of the Vernal NW quadrangle, Uintah County, Utah, and stratigraphic relationships of the Duchesne River Formation and Bishop Conglomerate: Provo, Utah, Brigham Young University, M.S. thesis, 68 p., 2 plate, scale 1:24,000.

Wen, S., and Nekvasil, H., 1994, SolvCalc—an interactive graphics program package for calculating the ternary feldspar solvus and for two-feldspar geothermometry: Computers & Geosciences, v. 20, p. 1025–1040, doi:10.1016/0098-3004(94)90039-6.

Winchester, J.A., and Floyd, P.A., 1977, Geochemical discrimination of different magma series and their differentiation products using immobile elements: Chemical Geology, v. 20, p. 325–343, doi: 10.1013/009-2541(77)90057-2.

Whitney, D.L., and Evans, B.W., 2010, Abbreviations for names of rock-forming minerals: American Mineralogist, v. 95, p. 184–187.

Wood, H.E., II, Chaney, R.W., Clark, J., Colbert, E.H., Jepsen, G. L., Reeside, J.B., Jr., and Stock, C., 1941, Nomenclature and correlation of the North American continental Tertiary: Geological Society of America Bulletin, v. 52, p. 1–48.

Woodburne, M.O., 2004, Late Cretaceous and Cenozoic mammals of North America: New York, Columbia University Press, 391 p.

Yonkee, W.A., and Weil, A.B., 2015, Tectonic evolution of the Sevier and Laramide belts within the North American Cordillera orogenic system: Earth-Science Reviews, v. 150, p. 531–593.

Zanazzi A., Kohn, M.J., MacFadden B.J., and Terry, D.O., Jr., 2007, Large temperature drop across the Eocene-Oligocene transition in central North America: Nature, v. 445, p. 639–642.

APPENDIX 1

Descriptions of Volcanic Ash Bed Samples

DRF-A (latitude 40.491478, longitude -109.746676). Light grayish-tan tuffaceous sandstone, 1 to 2 m thick with visible biotite grains when examined with a hand lens. This ash is distinct from all the other ashes in the field and is a moderately sorted, subrounded, poorly lithified sandstone with little clay. Contains biotite, sanidine, plagioclase, allanite, glass shards, zircon, magnetite, and detrital quartz grains. This is the only ash bed with coexisting plagioclase and sanidine. Laterally continuous where exposed. $^{40}Ar/^{39}Ar$ age from plagioclase of 39.5 Ma.

DRF-B (latitude 40.449856, longitude -109.720892). Light-gray clay matrix, 2 m thick with some visible biotite grains. Collected from middle Lapoint Member. Contains biotite, sanidine, and detrital grains including microcline. Laterally continuous where exposed.

DRF-C (latitude 40.417679, longitude -109.749658). Light- to medium-dark-gray clay matrix, 0.4 to 1 m thick, with abundant visible biotite grains. Highest tuff collected from Bobcat Ridge. Contains biotite, allanite, and detrital grains. Laterally continuous where exposed. Pictured to the right.

DRF-C ash

DRF-D (latitude 40.416545, longitude -109.746362). Medium- to dark-gray clay matrix, uppermost part of 5.5-m-thick tuff bed with some visible biotite grains. Collected from Bobcat Ridge. Poorly exposed due to erosion so lateral distribution is unknown. Contains biotite, apatite, zircon, and detrital grains.

DRF-E (latitude 40.416564, longitude -109.746445). Light- to medium-gray clay matrix, upper-middle part of 5.5-m-thick tuff bed with some visible biotite grains. Laterally continuous and used as contact between Lapoint and Dry Gulch Creek Members. Contains biotite and detrital grains.

DRF-F (latitude 40.416583, longitude -109.746469). Light- to medium-gray clay matrix, middle part of 5.5-m-thick tuff bed with some visible biotite grains. Laterally continuous and used as contact between Lapoint and Dry Gulch Creek Members. Contains biotite and detrital grains.

DRF-G (latitude 40.416519, longitude -109.746494). Light- to medium-gray clay matrix, lowermost part of 5.5-m-thick tuff bed with some visible biotite grains. Laterally continuous and used as contact between Lapoint and Dry Gulch Creek Members. Contains biotite and detrital grains including microcline. Pictured to the right.

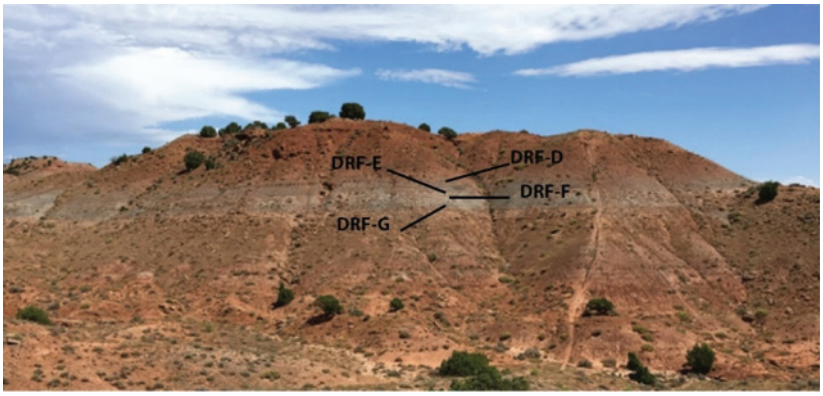

DRF-G ash

DRF-H (latitude 40.418116, longitude -109.747051). Light- to medium-gray clay matrix, 25 cm thick with abundant visible biotite

APPENDIX 1 (CONTINUED)

Descriptions of Volcanic Ash Bed Samples

grains. Lowest tuff bed from Bobcat Ridge and directly beneath Lapoint and Dry Gulch Creek contact. Poorly exposed so lateral distribution is unknown. Sampled from same tuff bed as DRF-I. Contains biotite, sanidine, allanite, titanite, and detrital grains including microcline.

DRF-I (latitude 40.418127, longitude -109.747087). Light- to medium-gray clay matrix, 25 cm thick with abundant visible biotite grains. Lowest tuff bed from Bobcat Ridge and directly below Lapoint and Dry Gulch Creek contact. Poorly exposed so lateral distribution is unknown. Sampled from same tuff bed as DRF-H. Contains biotite, sanidine, allanite, titanite, and detrital grains including microcline. $^{40}Ar/^{39}Ar$ age from sanidine of 39.36 ± 0.15 Ma.

DRF-J (latitude 40.409754, longitude -109.699966). Light- to medium-gray clay matrix, 27 cm thick, and some visible biotite grains. Collected from the upper Dry Gulch Creek Member. Poorly exposed so lateral distribution is unknown. Contains biotite, sanidine, and detrital grains. Pictured to the right.

DRF-J ash

DRF-K (latitude 40.397333, longitude -109.726184). Light- to medium-gray clay matrix, 25 cm thick with some biotite grains visible with a hand lens. Collected from the upper Dry Gulch Creek. Poorly exposed so lateral distribution is unknown. Contains biotite and detrital grains including microcline. Pictured below.

DRF-K ash

APPENDIX 2

Summary of Ages and Analytical Parameters

Complete $^{40}Ar/^{39}Ar$ Results

J-value:	0.0078199 ± 0.0000055 (2σ)	Instrument:	MAP 215-50
Sample:	DRF-H	Standard:	Fish Canyon sanidine
Material:	sanidine	Age (Ma):	28.201 ± 0.0460 Kuiper and others (2008)

$^{40}Ar \pm 1\sigma_{40}$	$^{39}Ar \pm 1\sigma_{39}$	$^{38}Ar \pm 1\sigma_{38}$	$^{37}Ar \pm 1\sigma_{37}$	$^{36}Ar \pm 1\sigma_{36}$	$\%^{40}Ar^*$	$^{40}Ar^*/^{39}Ar_K \pm 2\sigma$	K/Ca	Age ± 2σ	Included in wtd. mean
0.254487 ± 0.000237	0.087518 ± 0.000152	0.001032 ± 0.000031	0.000339 ± 0.000276	0.000026 ± 0.000003	96.89	2.817435 ± 0.012205	111.171	39.13 ± 0.34	✓
0.114178 ± 0.000204	0.039790 ± 0.000088	0.000446 ± 0.000019	0.000652 ± 0.000284	0.000005 ± 0.000003	98.74	2.833394 ± 0.025837	26.261	39.35 ± 0.71	✓
0.214451 ± 0.000220	0.075033 ± 0.000139	0.000924 ± 0.000010	0.000743 ± 0.000280	0.000007 ± 0.000003	99.01	2.829745 ± 0.013413	43.417	39.30 ± 0.37	✓
0.095063 ± 0.000219	0.032291 ± 0.000076	0.000352 ± 0.000020	0.000345 ± 0.000343	0.000017 ± 0.000003	94.57	2.784128 ± 0.028960	40.298	38.67 ± 0.80	✓
0.177620 ± 0.000226	0.062424 ± 0.000115	0.000755 ± 0.000025	0.000562 ± 0.000295	0.000002 ± 0.000003	99.59	2.833795 ± 0.015528	47.738	39.36 ± 0.43	✓
0.722795 ± 0.000370	0.089963 ± 0.000132	0.001042 ± 0.000020	0.000135 ± 0.000325	0.000013 ± 0.000003	99.47	7.991550 ± 0.016265	286.235	108.89 ± 0.43	
0.063918 ± 0.000185	0.019979 ± 0.000064	0.000233 ± 0.000015	0.000050 ± 0.000328	0.000023 ± 0.000003	89.14	2.851891 ± 0.046369	170.887	39.60 ± 1.27	✓
0.288660 ± 0.000259	0.062107 ± 0.000108	0.000710 ± 0.000030	0.000131 ± 0.000321	0.000029 ± 0.000003	96.98	4.507315 ± 0.017678	203.157	62.21 ± 0.48	
0.308759 ± 0.000259	0.031651 ± 0.000073	0.000401 ± 0.000012	0.000306 ± 0.000247	0.000096 ± 0.000003	90.69	8.846925 ± 0.039076	44.474	120.17 ± 1.03	
0.137580 ± 0.000203	0.042447 ± 0.000079	0.000509 ± 0.000014	0.000909 ± 0.000283	0.000036 ± 0.000003	92.14	2.986486 ± 0.023081	20.086	41.45 ± 0.63	
0.187762 ± 0.000251	0.065240 ± 0.000101	0.000741 ± 0.000015	0.000436 ± 0.000324	0.000006 ± 0.000003	99.08	2.851481 ± 0.014864	64.412	39.60 ± 0.41	✓
0.089866 ± 0.000203	0.031358 ± 0.000061	0.000380 ± 0.000018	0.000047 ± 0.000298	0.000000 ± 0.000003	99.84	2.861080 ± 0.031299	285.508	39.73 ± 0.86	✓
0.180430 ± 0.000211	0.048743 ± 0.000094	0.000605 ± 0.000028	0.000043 ± 0.000398	0.000013 ± 0.000003	97.83	3.621163 ± 0.020318	486.115	50.14 ± 0.56	
0.742268 ± 0.000377	0.072427 ± 0.000102	0.000879 ± 0.000027	0.000197 ± 0.000308	0.000012 ± 0.000003	99.51	10.198212 ± 0.020030	158.001	137.84 ± 0.52	
0.162617 ± 0.000218	0.056921 ± 0.000102	0.000767 ± 0.000017	0.000288 ± 0.000313	0.000003 ± 0.000003	99.41	2.840099 ± 0.018032	84.874	39.44 ± 0.50	✓
0.072944 ± 0.000219	0.025667 ± 0.000060	0.000309 ± 0.000023	0.000243 ± 0.000266	0.000006 ± 0.000003	97.63	2.774501 ± 0.038266	45.398	38.54 ± 1.05	✓
0.137531 ± 0.000224	0.047940 ± 0.000095	0.000565 ± 0.000015	0.000057 ± 0.000315	0.000002 ± 0.000004	99.59	2.857033 ± 0.026916	361.561	39.68 ± 0.74	✓
0.144788 ± 0.000219	0.050572 ± 0.000091	0.000587 ± 0.000015	0.000260 ± 0.000316	0.000001 ± 0.000003	99.80	2.857233 ± 0.020201	83.496	39.68 ± 0.56	✓
0.079638 ± 0.000200	0.027915 ± 0.000065	0.000358 ± 0.000019	0.000356 ± 0.000252	0.000001 ± 0.000003	99.79	2.846974 ± 0.034061	33.691	39.54 ± 0.94	✓
0.904683 ± 0.000534	0.082678 ± 0.000151	0.001034 ± 0.000020	0.000448 ± 0.000357	0.000016 ± 0.000003	99.48	10.885440 ± 0.023803	79.375	146.77 ± 0.62	
0.486829 ± 0.000323	0.042381 ± 0.000082	0.000516 ± 0.000022	0.000106 ± 0.000257	0.000003 ± 0.000003	99.83	11.467433 ± 0.032855	171.638	154.30 ± 0.85	
0.797324 ± 0.000464	0.075322 ± 0.000114	0.000914 ± 0.000021	0.000688 ± 0.000284	0.000047 ± 0.000004	98.23	10.398018 ± 0.021881	47.051	140.44 ± 0.57	
0.168151 ± 0.000241	0.052216 ± 0.000090	0.000626 ± 0.000039	0.000219 ± 0.000308	0.000001 ± 0.000003	99.90	3.216994 ± 0.018193	102.742	44.61 ± 0.50	
0.303205 ± 0.000306	0.033715 ± 0.000065	0.000400 ± 0.000022	0.000347 ± 0.000265	0.000012 ± 0.000003	98.81	8.886606 ± 0.032698	41.830	120.69 ± 0.86	
0.084988 ± 0.000177	0.019670 ± 0.000053	0.000236 ± 0.000012	0.000118 ± 0.000360	0.000001 ± 0.000003	99.53	4.300574 ± 0.049491	71.725	59.40 ± 1.35	
						weighted mean age (13 of 25):		39.36 ± 0.15	

Decay constants

λ_{40Ar}	$(0.580 \pm 0.014) \times 10^{-10}$ a^{-1}	Min and others (2000)
λ_{β^-}	$(4.884 \pm 0.099) \times 10^{-10}$ a^{-1}	Min and others (2000)
^{39}Ar	$(2.58 \pm 0.03) \times 10^{-3}$ a^{-1}	Stoenner and others (1965)
^{37}Ar	$(8.23 \pm 0.042) \times 10^{-4}$ h^{-1}	Stoenner and others (1965)
^{36}Cl	$(2.303 \pm 0.046) \times 10^{-6}$ a^{-1}	

Interfering isotope production ratios

$(^{40}Ar/^{39}Ar)_K$	0.00054 ± 0.00014	Jicha & Brown (2014)
$(^{38}Ar/^{39}Ar)_K$	0.01210 ± 0.00002	Jicha & Brown (2014)
$(^{39}Ar/^{37}Ar)_{Ca}$	0.000695 ± 0.00001	Renne and others (2013)
$(^{38}Ar/^{37}Ar)_{Ca}$	0.0000196 ± 0.000001	Renne and others (2013)
$(^{36}Ar/^{37}Ar)_{Ca}$	0.000265 ± 0.00002	Renne and others (2013)

Atmospheric argon ratios

$^{40}Ar/^{36}Ar$	298.56 ± 0.31	Lee and others (2006)
$^{38}Ar/^{36}Ar$	0.1885 ± 0.0003	Lee and others (2006)

APPENDIX 2 (CONTINUED)

Summary of Ages and Analytical Parameters

Complete $^{40}Ar/^{39}Ar$ Results

J-value:	0.0078199	± 0.0000055	(2σ)	Instrument:	MAP 215-50								
Sample:	DRF-H			Standard:	Fish Canyon sanidine								
Material:	sanidine			Age (Ma):	28.201 ± 0.0460	Kuiper and others (2008)							
	$^{40}Ar \pm 1\sigma_{40}$	$^{39}Ar \pm 1\sigma_{39}$		$^{38}Ar \pm 1\sigma_{38}$	$^{37}Ar \pm 1\sigma_{37}$	$^{36}Ar \pm 1\sigma_{36}$	$\%^{40}Ar^*$	$^{40}Ar^*/^{39}Ar_K \pm 2\sigma$	K/Ca	Age ± 2σ	Included in wtd. mean
	0.254487 ± 0.000237	0.087518 ± 0.000152		0.001032 ± 0.000031	0.000339 ± 0.000276	0.000026 ± 0.000003	96.89	2.817435 ± 0.012205	111.171	39.13 ± 0.34	✓
	0.114178 ± 0.000204	0.039790 ± 0.000088		0.000446 ± 0.000019	0.000652 ± 0.000284	0.000005 ± 0.000003	98.74	2.833394 ± 0.025837	26.261	39.35 ± 0.71	✓
	0.214451 ± 0.000220	0.075033 ± 0.000139		0.000924 ± 0.000010	0.000743 ± 0.000280	0.000007 ± 0.000003	99.01	2.829745 ± 0.013413	43.417	39.30 ± 0.37	✓
	0.095063 ± 0.000219	0.032291 ± 0.000076		0.000352 ± 0.000020	0.000345 ± 0.000343	0.000017 ± 0.000003	94.57	2.784128 ± 0.028960	40.298	38.67 ± 0.80	✓
	0.177620 ± 0.000226	0.062424 ± 0.000115		0.000755 ± 0.000025	0.000562 ± 0.000295	0.000002 ± 0.000003	99.59	2.833795 ± 0.015528	47.738	39.36 ± 0.43	✓
	0.722795 ± 0.000370	0.089963 ± 0.000132		0.001042 ± 0.000020	0.000135 ± 0.000325	0.000013 ± 0.000003	99.47	7.991550 ± 0.016265	286.235	108.89 ± 0.43	
	0.063918 ± 0.000185	0.019979 ± 0.000064		0.000233 ± 0.000015	0.000050 ± 0.000328	0.000023 ± 0.000003	89.14	2.851891 ± 0.046369	170.887	39.60 ± 1.27	✓
	0.288660 ± 0.000259	0.062107 ± 0.000108		0.000710 ± 0.000030	0.000131 ± 0.000321	0.000029 ± 0.000003	96.98	4.507315 ± 0.017678	203.157	62.21 ± 0.48	
	0.308759 ± 0.000259	0.031651 ± 0.000073		0.000401 ± 0.000012	0.000306 ± 0.000247	0.000096 ± 0.000003	90.69	8.846925 ± 0.039076	44.474	120.17 ± 1.03	
	0.137580 ± 0.000203	0.042447 ± 0.000079		0.000509 ± 0.000014	0.000909 ± 0.000283	0.000036 ± 0.000003	92.14	2.986486 ± 0.023081	20.086	41.45 ± 0.63	
	0.187762 ± 0.000251	0.065240 ± 0.000101		0.000741 ± 0.000015	0.000436 ± 0.000324	0.000006 ± 0.000003	99.08	2.851481 ± 0.014864	64.412	39.60 ± 0.41	✓
	0.089866 ± 0.000203	0.031358 ± 0.000061		0.000380 ± 0.000018	0.000047 ± 0.000298	0.000000 ± 0.000003	99.84	2.861080 ± 0.031299	285.508	39.73 ± 0.86	✓
	0.180430 ± 0.000211	0.048743 ± 0.000094		0.000605 ± 0.000028	0.000043 ± 0.000398	0.000013 ± 0.000003	97.83	3.621163 ± 0.020318	486.115	50.14 ± 0.56	
	0.742268 ± 0.000377	0.072427 ± 0.000102		0.000879 ± 0.000027	0.000197 ± 0.000308	0.000012 ± 0.000003	99.51	10.198212 ± 0.020030	158.001	137.84 ± 0.52	
	0.162617 ± 0.000218	0.056921 ± 0.000102		0.000767 ± 0.000017	0.000288 ± 0.000313	0.000003 ± 0.000003	99.41	2.840099 ± 0.018032	84.874	39.44 ± 0.50	✓
	0.072944 ± 0.000219	0.025667 ± 0.000060		0.000309 ± 0.000023	0.000243 ± 0.000266	0.000006 ± 0.000003	97.63	2.774501 ± 0.038266	45.398	38.54 ± 1.05	✓
	0.137531 ± 0.000224	0.047940 ± 0.000095		0.000565 ± 0.000015	0.000057 ± 0.000315	0.000002 ± 0.000004	99.59	2.857033 ± 0.026916	361.561	39.68 ± 0.74	✓
	0.144788 ± 0.000219	0.050572 ± 0.000091		0.000587 ± 0.000015	0.000260 ± 0.000316	0.000001 ± 0.000003	99.80	2.857233 ± 0.020201	83.496	39.68 ± 0.56	✓
	0.079638 ± 0.000200	0.027915 ± 0.000065		0.000358 ± 0.000019	0.000356 ± 0.000252	0.000001 ± 0.000003	99.79	2.846974 ± 0.034061	33.691	39.54 ± 0.94	✓
	0.904683 ± 0.000534	0.082678 ± 0.000151		0.001034 ± 0.000020	0.000448 ± 0.000357	0.000016 ± 0.000003	99.48	10.885440 ± 0.023803	79.375	146.77 ± 0.62	
	0.486829 ± 0.000323	0.042381 ± 0.000082		0.000516 ± 0.000022	0.000106 ± 0.000257	0.000003 ± 0.000003	99.83	11.467433 ± 0.032855	171.638	154.30 ± 0.85	
	0.797324 ± 0.000464	0.075322 ± 0.000114		0.000914 ± 0.000021	0.000688 ± 0.000284	0.000047 ± 0.000004	98.23	10.398018 ± 0.021881	47.051	140.44 ± 0.57	
	0.168151 ± 0.000241	0.052216 ± 0.000090		0.000626 ± 0.000039	0.000219 ± 0.000308	0.000001 ± 0.000003	99.90	3.216994 ± 0.018193	102.742	44.61 ± 0.50	
	0.303205 ± 0.000306	0.033715 ± 0.000065		0.000400 ± 0.000022	0.000347 ± 0.000265	0.000012 ± 0.000003	98.81	8.886606 ± 0.032698	41.830	120.69 ± 0.86	
	0.084988 ± 0.000177	0.019670 ± 0.000053		0.000236 ± 0.000012	0.000118 ± 0.000360	0.000001 ± 0.000003	99.53	4.300574 ± 0.049491	71.725	59.40 ± 1.35	
								weighted mean age (13 of 25):		39.36 ± 0.15	

Decay constants

λ_{-40Ar}	(0.580 ± 0.014) x 10^{-10} a^{-1}	Min and others (2000)
λ_{β^-}	(4.884 ± 0.099) x 10^{-10} a^{-1}	Min and others (2000)
^{39}Ar	(2.58 ± 0.03) x 10^{-3} a^{-1}	Stoenner and others (1965)
^{37}Ar	(8.23 ± 0.042) x 10^{-4} h^{-1}	Stoenner and others (1965)
^{36}Cl	(2.303 ± 0.046) x 10^{-6} a^{-1}	

Interfering isotope production ratios

$(^{40}Ar/^{39}Ar)_K$	0.00054 ± 0.00014	Jicha & Brown (2014)
$(^{38}Ar/^{39}Ar)_K$	0.01210 ± 0.00002	Jicha & Brown (2014)
$(^{39}Ar/^{37}Ar)_{Ca}$	0.000695 ± 0.00001	Renne and others (2013)
$(^{38}Ar/^{37}Ar)_{Ca}$	0.0000196 ± 0.000001	Renne and others (2013)
$(^{36}Ar/^{37}Ar)_{Ca}$	0.000265 ± 0.00002	Renne and others (2013)

Atmospheric argon ratios

$^{40}Ar/^{36}Ar$	298.56 ± 0.31	Lee and others (2006)
$^{38}Ar/^{36}Ar$	0.1885 ± 0.0003	Lee and others (2006)